Radiation trapping of the $^3P_1$-$^1S_0$ resonant transitions of xenon and krypton in Xe-Kr, Xe-Ar, and Kr-Ar mixtures: Kinetic analysis and determination of the van der Waals broadening coefficients

N. Sewraj, J. P. Gardou, Y. Salamero, and P. Millet

Centre de Physique des Plasmas, Université Paul Sabatier 31062 Toulouse, France

This work concerns radiation trapping of the 123-nm krypton and 147-nm xenon lines, in the presence of a lighter rare gas, as well as the study of the decay processes of the relevant resonant states due to inelastic collisions. It deals with Kr-Ar, Xe-Kr, and Xe-Ar mixtures. Pulsed, brief selective excitation of the Xe($^3P_1$) or Kr($^3P_1$) resonant states by three-photon absorption was achieved by means of a tunable dye laser. Spectral and temporal analysis was then performed. The time resolved luminescence, filtered in the vacuum ultraviolet region, obeys a decay law described by the sum of two exponential terms which are attributed to the deexcitation of the $^3P_1$ and $^3P_2$ states. The decay constants are estimated by the maximum likelihood method applied to a Poisson statistical law. In order to correctly determine the collision rate constants, it is important to account for variations of the apparent lifetime according to the gas concentration. Analysis of both systematic experimental errors and statistical errors leads to a good estimation of the accuracy of the results obtained. For each mixture, the variation of the time constants as a function of partial pressures allows a determination of the resonance broadening coefficient and van der Waals broadening coefficient of the transition studied, as well as the two- and three-body inelastic collision rates relative to the $^3P_1$ and $^3P_2$ states. There exists no energy transfer between the two gases. For binary rare-gas mixtures, where only the heavier gas is excited, homonuclear and heteronuclear three-body reactions account for the decay of the $^3P_1$ state. Nevertheless, for the $^3P_2$ state we observe both two- and three-body collisions. In order to simulate resonance radiation trapping, a numerical method based upon Monte Carlo techniques was used. Calculations were first performed and validated for an infinite cylinder. The difference between calculation and experiment was less than 1%. Then the program was adapted to our real experimental conditions and applied to the binary mixtures studied. A good agreement was found between experiments and calculations. Furthermore, our program allows us to obtain information not easily obtained experimentally.

PACS number(s): 32.80.−t, 32.70.Cs, 32.50.+d, 32.70.Jz

I. INTRODUCTION

This work is part of a more general study of binary mixtures of rare gases, selectively excited in a given atomic or molecular state in order to determine the decay and formation rate constants of the various reaction products [1–3]. Resonant states play an important role in excimer formation and are involved in UV sources based on rare gases. Atoms excited in a resonant state will decay to the ground level by emission of resonant photons themselves having a good probability of being absorbed by surrounding ground-state atoms, and then reemitted. This radiation trapping, which has not been studied much in rare-gas mixtures, is often used either to transfer energy between rare gases or to improve the characteristics of a gas discharge. The present paper thus deals with trapping of xenon and krypton resonance radiation in pure gases and in several binary mixtures, and the simultaneous determination of the relevant decay rates by collision.

In rare-gas mixtures, most previous studies, have dealt with energy transfer, which is very efficient when it occurs from a lighter rare gas towards a heavier one. This type of transfer was first demonstrated by Gedanken *et al.* [4] in 1972. The interpretation of such results is not easy, due to the frequent overlaps of the observed emissions. Nonetheless, very few works [5,6] used selective excitation to simplify the initial conditions. Even in mixtures where these transfers are unlikely, the decay of the resonant states by collision is favored by radiation trapping processes, which may make them competitive with photon emission. It is also essential to account for the variation of the apparent lifetime, in order to correctly determine the collision rate constants relative to these resonant states, in particular when the excimer formation rate constants are deduced from analysis of the resonant or first continuum emission. Although the trapping phenomenon was widely investigated in pure rare gases both experimentally [7,8] and theoretically [7,9–11] it was little studied in gas mixtures [12]. Unlike in works concerning energy transfer between rare gases, we sought an initial excitation of the heaviest gas in its first resonant state, thus avoiding energy transfer toward the lighter gas, whose first energy levels are higher. In such conditions, additional broadening of the resonance line is shown to be caused by the lighter rare gas. Our results also show that the lighter gas contributes to the collisional decay of the resonant state.

A. Formulation of resonance radiation trapping

The process of photon emission and reabsorption, which goes on until the photon reaches the walls of the enclosing vessel, is at the origin of resonance radiation trapping. The escape factor *g*, which characterizes this radiation trapping, is defined as the inverse of the mean number of absorption-

reemission processes, and depends on both the gas used and the geometrical characteristics of the experimental device. It allows the apparent lifetime τ_a to be expressed as a function of the natural lifetime τ_n:

$$\tau_a = \frac{\tau_n}{g} \tag{1}$$

Resonance radiation trapping was first formulated by Holstein [9,10] and Biberman and Aksperim [13], who showed that the resonant state density $n(\vec{r},t)$ obeys an integrodifferential equation. Their works became the basis of many studies by different authors like Payne and co-workers [7,11] and in Ref. [14]:

$$\frac{\partial n(\vec{r},t)}{\partial t} = S(\vec{r},t) - \frac{1}{\tau_n} n(\vec{r},t) - F_C n(\vec{r},t)$$

$$+ \frac{1}{\tau_n} \int_{volume} n(\vec{r}',t) G(\vec{r}',\vec{r}) dv'. \tag{2}$$

In Eq. (2), the loss terms correspond to the radiative decay of the excited states and the decay by collision of these states with the frequency F_c. There are two source terms: the first, $S(\vec{r},t)$, represents the creation rate of excited states at time t, whereas the second describes the variation of density due to the reabsorption at $\vec{r}$ of photons emitted in the cell. The term $G(\vec{r}',\vec{r}) dv'$ is the probability that a photon emitted at $\vec{r}'$ in the elementary volume dv' is absorbed at $\vec{r}$.

Holstein assumed isotropic photon emission and complete frequency redistribution. Complete frequency redistribution means that no correlation exists between the frequency of the absorbed and emitted photons if at least one elastic collision occurs with the excited atom before it emits a photon. However, his calculations only hold for an optically thick medium, that is $k(\nu_0)R \gg 1$ [where $k(\nu_0)$ is the absorption coefficient of the resonance transition at the central frequency ν_0, and R the characteristic dimension of the vessel].

In the simple case where a short duration pulsed source is used, and if inelastic collisions may be neglected, the general solution of the equation is a discrete sum of exponential terms:

$$n(\vec{r},t) = \sum_i C_i m_i(\vec{r}) \exp\left(-g_i \frac{t}{\tau_n}\right) \approx C m(\vec{r}) \exp\left(-g \frac{t}{\tau_n}\right). \tag{3}$$

C_i and C are constants depending on initial conditions. Late in the decay time, the lowest value g of the parameters g_i determines the decay rate of the excited-state density. This escape factor g, which is dependent on the cell shape, were calculated by Holstein for two ideal geometries: an infinite slab and an infinitely long cylinder of radius R. Each calculation set was carried out with either Doppler or pressure broadening. Here we only give the escape factor g for a cylindrical geometry, which is closest to our experimental setup, for Doppler broadening [Eq. (4)] and pressure broadening [Eq. (6)], as a function of the absorption coefficient k at the central frequency ν_0 (or wavelength λ_0):

(a) *Doppler broadening*:

$$g = \frac{1.60}{k_D(\nu_0)R \sqrt{\pi \ln[k_D(\nu_0)R]}} \tag{4}$$

with

$$k_D(\nu_0) = \frac{\lambda_0^3}{8\pi^{3/2}} \frac{g_2}{g_1} \frac{1}{\tau_n} \left(\frac{m}{2kT}\right)^{1/2} N_0. \tag{5}$$

(b) *Pressure broadening*:

$$g = \frac{1.115}{\sqrt{\pi k_p(\nu_0)R}} \tag{6}$$

with

$$k_p(\nu_0) = \frac{\lambda_0^2}{4\pi^2} \frac{g_2}{g_1} \frac{1}{\tau_n \Delta\nu} N_0 \tag{7}$$

In formulas (5) and (7), g_2 and g_1 are respectively the statistical weights of the resonant and ground states, N_0 is the density of ground state atoms, and $\Delta\nu$ is the full width at half maximum (FWHM) of the local line profile.

The predominant broadening phenomenon corresponds to the lowest apparent lifetime, and so to the greatest escape factor. In the cylindrical configuration, the lower limit of the pressure broadening domain can be deduced from the comparison of Eq. (4) with Eq. (6). Figure 1 shows that it is about 10^{-2} Torr for both krypton and xenon. It follows that for our experimental pressure range (0.2–1000 Torr), we can account for only pressure broadening. Moreover, the impact approximation is also valid in this domain. Indeed, for pressures lower than about ten atmospheres, the collision time lasts less than the duration between two collisions [15,16].

B. Resonance radiation trapping in a binary mixture with pressure broadening

Let us examine a binary mixture X-Y where gas X is excited on its $^3P_1$ resonant state. Homonuclear (X-X) and heteronuclear collisions (X-Y) lead to resonance broadening and van der Waals broadening both having a Lorentzian absorption profile, respectively. For homonuclear collisions the resonance absorption coefficient $k_X(\nu)$ depends on the FWHM $\Delta\nu_X$ which is directly proportional to the density of disturbing atoms N_{0X}. In Eq. (10), ξ_X is the resonance broadening coefficient of the transition,

$$k_X(\nu) = \frac{k_X(\nu_0)}{1 + [4(\nu-\nu_0)^2/\Delta\nu_X^2]} \tag{8}$$

with

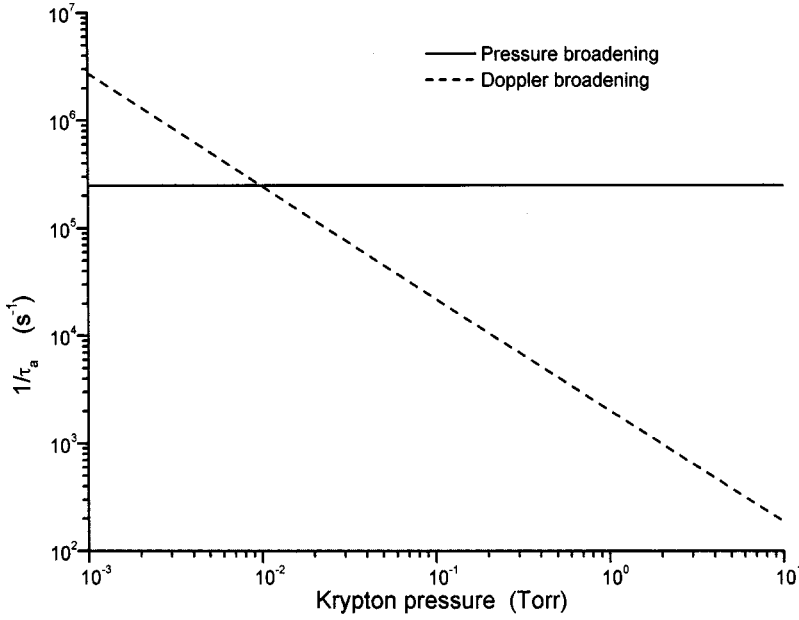$$k_X(\nu_0) = \frac{\lambda_0^2}{4\pi^2} \frac{g_2}{g_1} \frac{1}{\tau_n \Delta\nu_X} N_{0X} \tag{9}$$

and

FIG. 1. Pressure dependence of the calculated Kr($^3P_1$) radiative decay frequency in krypton for Doppler and pressure broadening.

$$\Delta \nu_X = 2 \xi_X N_{0X}. \tag{10}$$

For heteronuclear collisions, the van der Waals absorption coefficient $k_Y(\nu)$ is described by an expression similar to Eq. (8). Its FWHM $\Delta \nu_Y$ is given by

$$\Delta \nu_Y = 2 \xi_Y N_{0Y}, \tag{11}$$

where ξ_Y is the van der Waals broadening coefficient. The overall absorption coefficient $k_T(\nu)$ of the line, accounting for both types of broadening, is the convolution product of $k_X(\nu)$ and $k_Y(\nu)$ since the two effects are independent: $k_T(\nu)$ is therefore Lorentzian too, and its FWHM is given by $\Delta \nu_T = \Delta \nu_X + \Delta \nu_Y$. The absorption coefficient at the line center is thus

$$k_T(\nu_0) = \frac{\lambda_0^2}{4\pi^2} \frac{g_2}{g_1} \frac{1}{\tau_n \Delta \nu_T} N_{0X} = \frac{\lambda_0^2}{8\pi^2} \frac{g_2}{g_1} \frac{1}{\tau_n} \frac{N_{0X}}{\xi_X N_{0X} + \xi_Y N_{0Y}}. \tag{12}$$

In a mixture, for the infinite cylinder (Sec. I A) with pressure broadening, the apparent lifetime [Eq. (1)] is obtained by replacing k_P in Eq. (6) by k_T [Eq. (12)]:

$$\tau_a = \frac{\lambda_0}{1.115\sqrt{8\pi}} \left(\frac{g_2}{g_1} R \tau_n \right)^{1/2} \left(\frac{N_{0X}}{\xi_X N_{0X} + \xi_Y N_{0Y}} \right)^{1/2}. \tag{13}$$

This depends only on the ratio of the partial pressures P_X and P_Y, and can thus be expressed in terms of the concentration $C = P_Y / (P_Y + P_X)$ of the foreign gas:

$$\tau_a = \frac{\lambda_0}{5.59} \left(\frac{g_2}{g_1} R \tau_n \right)^{1/2} \left(\frac{1-C}{(1-C)\xi_X + C\xi_Y} \right)^{1/2}. \tag{14}$$

In a pure gas, the apparent lifetime is independent of the pressure, whereas in a mixture it remains independent of the total pressure only at constant concentration.

In our experimental conditions, where the enclosing vessel has a complex shape, an analytic calculation of the escape factor cannot be achieved. However, the variation law of the apparent lifetime following the concentration should remain similar to Eq. (14) if pressure broadening predominates and if the impact approximation still stays valid, as shown in the Appendix. One of our objectives is to experimentally verify the validity of relation (15):

$$\frac{1}{\tau_a} = \frac{1}{A} \left(\xi_X + \frac{C}{1-C} \xi_Y \right)^{1/2}. \tag{15}$$

Furthermore, the estimation of the parameters of a linear fit of $1/\tau_a^2$ versus $C/(1-C)$ allows the ratio ξ_Y/ξ_X to be obtained, even though constant A, which takes into account the implied transition as well as the geometric configuration of the cell, cannot be calculated in our experimental conditions. The van der Waals broadening coefficient ξ_Y can be obtained since we can use the theoretical expression of ξ_X,

$$\xi_X = \frac{K}{2} \left(\frac{g_1}{g_2} \right)^{1/2} \frac{f}{2\pi \nu_0 m} \frac{e^2}{4\pi\varepsilon_0}, \tag{16}$$

where f is the absorption oscillator strength of the transition, m and e are the mass and the charge of the electron, and K is the constant of the resonance interaction. In order to determine ξ_X, we need either the oscillator strength of the transition or the natural lifetime. There exist very few direct measurements of the natural lifetime τ_n of the resonant state (these must be made at very low pressures, between 10^{-6} and 10^{-5} Torr [17]). The oscillator strength can also be determined by an absorption method. The diversity of the values found in the literature (Table I and II) led us to adopt our own determination, deduced from our measurement of the apparent lifetime τ_a, since the escape factor of our experimental device is obtained from our simulation program of resonance radiation trapping. The resonance interaction constant K has been subjected to numerous theoretical and ex-

TABLE I. Absorption oscillator strength values for the $Kr(^3P_1) \rightarrow Kr(^1S_0)$ transition at 123.6 nm

f	Reference	f	Reference	f	Reference
0.208	[17]	0.166	[54]	0.204	[60]
0.18	[49]	0.175±0.005	[55]	0.21	[61]
0.214	[50]	0.1775±0.0050	[56]	0.158	[62]
0.143	[51]	0.17	[57]	0.204	[63]
0.155	[52]	0.195	[58]		
0.21	[53]	0.187	[59]	0.173±0.009	This work

TABLE III. Experimental and theoretical determinations of the resonance interaction constant K.

K (experiment)	Reference	K (theory)	Reference	K (theory)	Reference
1.96±0.12	[30]	2.08	[15]	2.07	[24]
2.08±0.28	[31]	1.97	[18]	2.08	[25]
2.0±0.10	[32]	1.81	[19]	1.81	[26]
2.25±0.15	[33]	2.31	[20]	2.07	[27]
2.3±0.20	[34]	2.72	[21]	2.43	[28]
2.15±0.15	[49]	2.72	[22]	2.01	[29]
		1.81	[23]	1.93	[89]

perimental determinations, and the values differ significantly; some of these discrepancies were analyzed by Omont [18]. In Table III, the experimental values spread between 1.95 and 2.3. Thus we retained $K = 2.1 \pm 0.1$, which corresponds to the mean and the standard deviation of the experimental values.

II. MODELING IN AN INFINITELY LONG CYLINDER BY THE MONTE CARLO METHOD

In our actual experimental conditions, the main utility of a model resides in the difficulty to analytically solve the radiation transfer equation (2) in order to determine the spatial and temporal evolution of the resonant state densities. The Monte Carlo method allows the reconstitution of the whole phenomenon by following the evolution of the excited atoms consecutive to the initial excitation. This simulation, suited to our experimental apparatus, can also allow the evaluation of the influence of various parameters, such as the location of the resonant states initially created, on the temporal decay of the luminescence. The photon-collecting conditions can be optimized, and we can also obtain the spectrum of the emitted line which cannot be recorded due to the low light fluxes involved. Finally, this model can be extended to various binary mixtures of rare gases.

Our objective here is first to describe and then to validate the method for an ideal setup, namely, the infinitely long cylinder where the results can be compared to those obtained from Holstein's theory. In Sec. V, we will describe how this method can be adapted to our experimental device in order to calculate the escape factor. The natural lifetime can then be determined from the measurement of the apparent lifetime.

A. Principle of the method

The transfer of the excitation energy of an atom is followed step by step from the initial excitation on a $^3P_1$ resonant state until the photon leaves the cell. The parameters which characterize the emitted photon are (i) the emission instant t_e of a photon and its frequency ν_e following a Lorentzian profile, and (ii) the emission direction described by two angles θ and φ and the distance D covered between the emission and absorption points (Fig. 2).

For each emission process, all five variables described above are evaluated by an integral method from random numbers x_i uniformly distributed over the interval [0;1]. This calculation is done again and again until a photon leaves the cell. In order to obtain satisfactory statistical accuracy, the procedure is repeated for an initial number of excited states between 10^5 and 10^6.

Determination of the frequency ν_e. In our experimental conditions, pressure broadening is dominant, and leads to a normalized Lorentzian profile $P(\nu)$. Since the partial pressure of the excited gas is always greater than 0.2 Torr for xenon and 1 Torr for krypton, the emission and absorption frequencies of the photons are independent of each other, and we can assume complete frequency redistribution [7]. The uniformly distributed random number x_1 is linked to the frequency ν_e of the emitted photon:

$$x_1 = \int_{-\infty}^{\nu} P(\nu) d\nu = \int_{-\infty}^{\nu} \frac{2}{\pi \Delta \nu} \frac{1}{1 + [4(\nu - \nu_0)^2 / \Delta \nu^2]} d\nu. \tag{17}$$

So

TABLE II. Absorption oscillator strength values for the $Xe(^3P_1) \rightarrow Xe(^1S_0)$ transition at 146.9 nm.

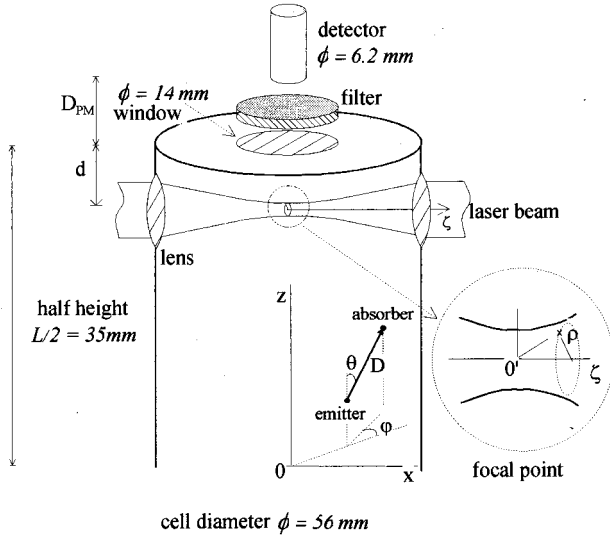| f	Reference	f	Reference	f	Reference
0.263	[17]	0.26	[65]	0.226	[70]
0.26±0.01	[49]	0.214	[66]	0.244	[71]
0.27	[53]	0.183	[67]	0.26	[72]
0.26	[58]	0.256±0.008	[68]	0.222	[73]
0.28	[64]	0.264±0.016	[69]	0.273	[50]
				0.244±0.012	This work

FIG. 2. Schematic diagram showing the analysis cell and the laser beam, used for modeling.

$$\nu_e = \nu_0 + \frac{\Delta \nu_T}{2} \tan[\pi(x_1 - 0.5)]. \qquad (18)$$

Emission time t_e. If τ_n is the natural lifetime of the resonant state, the probability that the atom emits a photon between t_e and $t_e + dt$ is $\exp(-t_e/\tau_n)(dt/\tau_n)$. We associate a random number x_2 to the density of probability that a photon is emitted before t_e:

$$t_e = -\tau_n \ln(1 - x_2). \qquad (19)$$

Emitting angles φ and θ. Assuming photon emission is isotropic, the emitting direction is given by the azimuthal angle $\varphi (0 \le \varphi < 2\pi)$ and polar angle $\theta (0 \le \theta \le \pi)$ to which the uniformly distributed random numbers x_3 and x_4 are associated:

$$\varphi = 2\pi x_3 \qquad (20)$$

and

$$\cos\theta = 1 - 2x_4. \qquad (21)$$

Distance D covered between two collisions. Let $T(D,\nu) = \exp[-k(\nu)D]$ be the probability that a photon covers distance D without being absorbed. D can be associated to a uniformly distributed random number x_5:

$$D = -\frac{1}{k(\nu)} \ln(x_5). \qquad (22)$$

If the photon is absorbed inside the vessel, then the absorption point becomes the new emission point, and the above process is repeated. If not, the photon is absorbed by the inner walls and an excited state disappears from the cell. Its frequency, its exit time, and the number of absorption-reemission processes are memorized. A new initially excited resonant state is then considered, and the treatment repeated

TABLE IV. Comparison between corrected theoretical and calculated values of the inverse of the escape factor.

	$1/g$ (modified Holstein relation)	$1/g$ (obtained from the model)	Difference
$R = 5.25$ mm	1046	1045	0.1%
$R = 10$ mm	1443	1442	0.07%
R=28 mm	2415	2403	0.5%

until all the initial resonant states are worked out. The mean value of the number of absorption-reemission processes, for all initial resonant states, is the inverse of the escape factor g.

B. Application to an infinitely long cylinder

This study is applied to the $Kr(^3P_1) \rightarrow Kr(^1S_0)$ resonance line for a cylindrical geometry, assuming pressure broadening. Simulations have been performed on 10^6 resonant states. The statistical fluctuations have been evaluated for ten sets of random numbers. The relative deviations on the escape factor are less than 0.7%.

The cylinder should be long enough compared to its radius: when the length of the cylinder is at least 20 times greater than its radius, our results show that the escape factor variations are smaller than the statistical fluctuations. Finally, calculations were done for three different cylinder radii: 5.25, 10, and 28 mm.

The difference between the simulated values and those deduced from Holstein's equation (6) did not exceed 1.4%; however, this is greater than statistical fluctuations. In addition, the values obtained from our model were always less than Holstein's. According to Payne and Cook [11], the numerical coefficient present in the numerator of Eq. (6) would be worth 1.125 instead of 1.115. The corrected value of the coefficient leads to a smaller number of absorption-reemissions which is very close to ours (Table IV).

III. EXPERIMENTAL SETUP

A. Laser source, analysis cell, and detection device

Our experimental setup was designed to record luminescence following selective population of the resonant states by three-photon excitation, using a tunable dye laser. Here we only briefly describe the main features of the experimental device, whose principal [1] and latest developments [35,36] were already extensively reported.

The selective excitation of $Xe(^3P_1)$ was performed with an energy of about 50 μJ at a wavelength of 440.9 nm, using coumarin C440 dye. For $Kr(^3P_1)$, an energy of about 12 μJ at 370.8 nm was obtained with PBD dye. The spectral width of the laser beam was about 0.5 cm^{-1}. We obtained 5 ns duration impulses, at a frequency of 50 Hz.

The laser beam enters a cylindrical stainless steel chamber radially, and is focused on the cell's axis by means of a plane-convex 40-mm lens (Fig. 2). Excitation is performed at a small volume compared to that of the cell. In order to check that multiphotonic ionization did not occur, a Keithley electrometer was used.
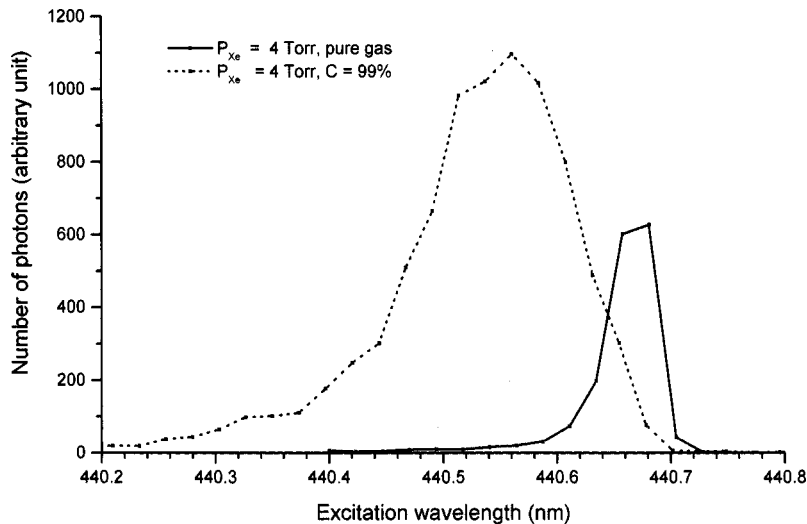
FIG. 3. Excitation spectra for the 147-nm emission in pure xenon and a Xe-Kr mixture.

Before filling, the cell was pumped down to about 10^{-7} Torr with an ionic pump. While the cell was being filled up, the gases were further purified by drifting them through an aluminum-zirconium getter pump. The gas pressure was measured by a ''Datametrics'' Barocell-type capacitive manometer using two sensors covering the 10^{-1}–10-Torr and 10–1000-Torr domains.

Luminescence was observed perpendicularly to the laser beam by means of a vacuum ultraviolet (VUV) photomultiplier (EMR 510G Extremely Solar Blind) through a magnesium fluoride porthole centered on the axis of the cell. The distance from the center of the excited volume to the window can be modified with a micrometer but in most experiments, it was equal to 1.40 ± 0.05 mm. The wavelength was selected by either a VUV Mc Pherson 218 monochromator for the recording of the emission spectra, or an interferential filter for the excitation spectra and the time-dependent studies.

B. Temporal analysis of the afterglow luminescence

At its exit, the laser beam falls upon a fast photodiode which provides the initial instant for each laser pulse. The number of photons as well as their instant of detection are stored in a multichannel Stanford Research SR 430 analyzer set for 16 384 channels and 5-ns resolution. In our conditions of low detected luminous flux, the histograms recorded include both a great number of channels and a low counting rate per channel. The least-squares method therefore converges with difficulty, and also introduces systematic errors. In order to determine the temporal evolution law, we developed a maximum likelihood data processing method applied to a Poisson distribution. The accuracy of all our results, apparent lifetime, collision rate constant, and broadening coefficients, was simultaneously evaluated for both statistical and systematic errors. In the former case a Monte Carlo method was used, whereas for systematic errors we used a classical uncertainty calculation applied to the estimation of the coefficients by the least-squares method [35].

C. Presentation of the excitation spectra

In order to determine the most favorable excitation conditions, an excitation spectrum was recorded before the temporal analysis. For example, excitation spectra obtained in pure xenon and in a xenon-krypton mixture are shown in Fig. 3. When the pressure is equal to 4 Torr, the excitation domain is relatively narrow since it is of the atomic type for low xenon pressures: $\mathrm{Xe}(^1S_0) + 3h\nu_{\mathrm{laser}} \rightarrow \mathrm{Xe}(^3P_1)$. For higher pressures, in both the pure gas and the mixtures, a broad component corresponds to the excitation of the $\mathrm{Xe}_2[1_u(^3P_1)]$ state from dimers in the ground state: $\mathrm{Xe}_2[0_g^+] + 3h\nu_{\mathrm{laser}} \rightarrow \mathrm{Xe}_2[1_u(^3P_1)]$. This weakly bound excited state rapidly dissociates, and leads to an initial population of $\mathrm{Xe}(^3P_1)$ atoms. The shift of maximum intensity toward shorter wavelengths with increasing pressure is certainly related to the third-harmonic generation. Indeed, the maximum of the generated radiation intensity occurs at shorter wavelengths when the pressure increases: $\mathrm{Xe}_2[0_g^+] + h\nu_{\mathrm{generated}} \rightarrow \mathrm{Xe}_2[1_u(^3P_1)]$.

Figure 3 also illustrates the influence of krypton on the excitation conditions of $\mathrm{Xe}(^3P_1)$. One may refer to some more thorough works done in our laboratory for further information concerning the excitation spectra of rare gases [37,38] and the involvement of the third harmonic of the laser beam [39,40].

IV. EXPERIMENTAL RESULTS IN PURE KRYPTON

Though many kinetic studies have been done for $\mathrm{Kr}(^3P_1)$ in pure gas, the dispersion of the values of the natural lifetime and of the kinetic constants led us to do new measurements. Our experimental pressure domain [1; 70 Torr] was chosen to observe either the first resonance line or the first continuum resulting from the deexcitation of $\mathrm{Kr}_2[0_u^+(^3P_1)]$, for which the resonant state is a precursor. The luminescence was observed behind an interferential filter centered at 128 nm, and whose FWHM is 10 nm. A time-resolved analysis was performed with a time resolution of 5 ns over a range of 81 μs.

For pressures lower than 15 Torr, luminescence decay is well described by a single exponential term. For higher pressures, a second term appears; its amplitude increases with the krypton pressure. Due to the inaccuracies arising from its low amplitude, we will not present the results concerning the
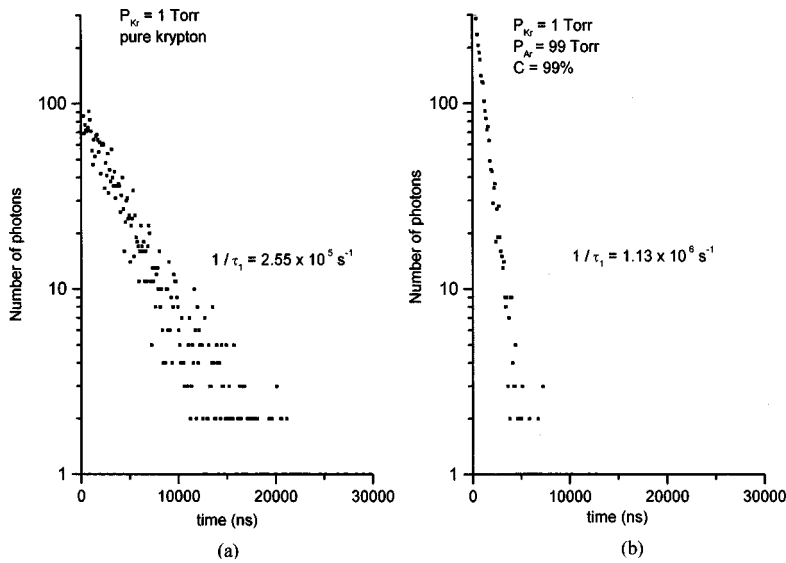
FIG. 4. Experimental record of temporal decay of the Kr($^3P_1$) in pure krypton and a Kr-Ar mixture. (For the sake of clarity, histograms recorded with a resolution of 5 ns are integrated and presented with 100 ns).

second term here. The same phenomenon is more clearly observed in xenon (Sec. VII) over a broader range of pressures, and the Xe($^3P_2$) metastable has been clearly identified. Thus, here we can reasonably attribute this weak exponential term to the decay of the Kr($^3P_2$) state. Taking this second term into account in our data processing allowed us to analyze Kr($^3P_1$) decay with a good accuracy up to 70 Torr.

An experimental histogram obtained at 1 Torr is represented in Fig. 4(a), while Fig. 5 shows the variation of the decay frequency $1/\tau_1$ versus P_{Kr}^2. The most general form of the decay rate in krypton is given by

$$\frac{1}{\tau} = k_1 + k_2 P_{Kr} + k_5 P_{Kr}^2. \tag{23}$$

The constants k_i of Eq. (23) are determined by the least-squares method. To each point we assign a statistical weight determined by the standard deviation of the values of $1/\tau_1$

obtained by working out thirty simulated histograms by a Monte Carlo method. Consideration of the binary collisions leads to a negative value of k_2, which is marred by an uncertainty of over 100%. Examination of Fig. 5 confirms the quadratic variation of the decay frequency with the krypton pressure. Over the whole pressure range we applied the expression

$$\frac{1}{\tau_1} = k_1 + k_5 P_{Kr}^2, \tag{24}$$

with $k_1 = (2.44 \pm 0.02) \times 10^{+5}$ s^{-1} and $k_5 = 116 \pm 7$ Torr^{-2} s^{-1}. The apparent lifetime deduced from coefficient k_1 is equal to 4.09×10^{-6} s. Constant k_5 expresses the three-body collision reaction
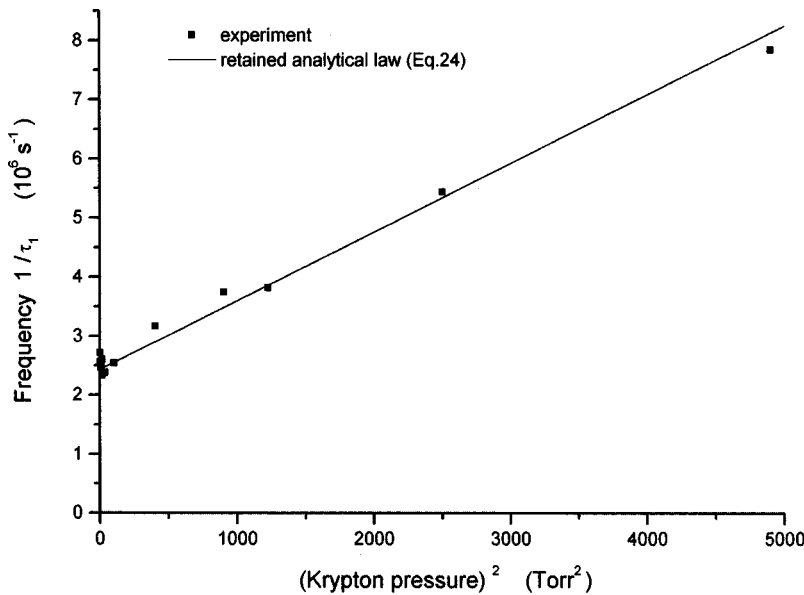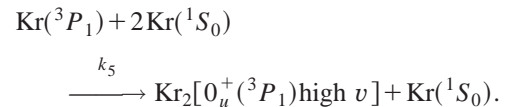
$$\text{Kr}(^3P_1) + 2\,\text{Kr}(^1S_0)$$

$$\xrightarrow{k_5} \text{Kr}_2[0_u^+(^3P_1)\text{high } v] + \text{Kr}(^1S_0).$$

FIG. 5. Variation of the Kr($^3P_1$) decay frequency in pure krypton as a function of P_{Kr}^2.

TABLE V. Two- and three-body rate constants relative to the decay of $Kr(^3P_1)$ in pure krypton.

K_2 (Torr^{-1} s^{-1})	k_5 (Torr^{-2} s^{-1})	Reference	k_2 (Torr^{-1} s^{-1})	k_5 (Torr^{-2} s^{-1})	Reference
1940	70.8	[38]		25.5	[44]
	31.3	[41]	355	1.76	[45]
	37	[42]	2050	82	[46]
7970	8.45	[43]		116±7	This work

Table V summarizes the two- and three-body rate constants of the $Kr(^3P_1)$ state obtained by various authors. Among recent works, those of Audouard *et al.* [41] and Kerdoussi [38] used selective excitation. The disagreement with Audouard *et al.*'s results could simply arise from a divergence of interpretation of concordant experimental results. The results of Kerdoussi were previously obtained in the same geometrical and excitation conditions as ours, the main difference being the absence of the binary collision term in our case.

The improvement of the resolution and of the dynamics of our recording system as well as the lower pressures we used, account for the fact that our results are less influenced by the presence of the second exponential term. New processing of Kerdoussi's results, up to only 60 Torr, gave an expression close to ours: $1/\tau_1 = 3.02 \times 10^5 + 110 P_{Kr}^2$.

The radiative decay of the molecular $0_u^+[^3P_1]$ state contributes to the well known emission of the first continuum. In addition, our exploitation should have also led to another exponential term corresponding to the radiative lifetime of the molecular state. However, according to Audouard *et al.*'s [41] and Bonifield *et al.*'s [42] works, this lifetime is about 4 ns and the time resolution (5 ns) of our recording device cannot allow its determination.

V. MODELING OF RADIATION TRAPPING UNDER OUR EXPERIMENTAL CONDITIONS

The influence of an added gas on the apparent lifetime should allow us to determine the broadening coefficient ξ_Y of the line, due to this gas. As we already mentioned in Sec. I B, the oscillator strength should first be determined. It can be deduced from the measured apparent lifetime in the pure gas and the calculated escape factor obtained by our radiation trapping model. The program should therefore be suited to our experimental setup. Our experiment was modeled taking into account only pressure broadening, which in fact corresponds to our experimental results obtained over the pressure range [0.2; 70 Torr].

A. Initial creation of the resonant states

As shown in Fig. 2, the excited species are located in the cell with a cylindrical system of coordinates (O, r, φ, z) where the axis (Oz) is given by the vessel's axis itself. The excited states are initially created by the laser beam focused on this axis, close to the observation porthole ($d = 1.40 \pm 0.05$ mm). The axially symmetric laser beam is assumed to be radially Gaussian, and to remain so after focusing. The initial distribution of the resonant states created by the laser beam can be calculated using the local system of cylindrical coordinates (O', ρ, ψ, ζ) centered on the focus with the axis $(O'\zeta)$ in the beam direction. The number of resonant states created by three-photon absorption in elementary volume dv is

$$dn(\rho, \zeta) = \sigma^{(3)} I^3 N_0 dv, \qquad (25)$$

where $\sigma^{(3)}$ represents the three-photon excitation cross section, I the local intensity of the laser beam, and N_0 the density of ground state atoms. For a focused Gaussian beam, the number of resonant states created can be expressed as

$$dn(\rho, \zeta) = \frac{K}{[1+(\zeta/\zeta_0)^2]^3} \exp\left[\frac{-6\rho^2}{w_0^2[1+(\zeta/\zeta_0)^2]}\right] dv \qquad (26)$$

with

$$\zeta_0 = \frac{b}{2} = \frac{\pi w_0^2}{\lambda_0}, \qquad (27)$$

where w_0 is the beam waist and b the confocal parameter. In our conditions, $w_0 = 15\ \mu$m and $b = 150\ \mu$m. The resonant states are distributed according to the above defined density, by drawing three random numbers x_6, x_7, and x_8, respectively, associated with the coordinates ρ, ψ, and ζ. $x_6 = \rho$ is a random number having a Gaussian distribution, x_7 and x_8 are uniformly distributed over $[0;1]$, and x_7 corresponds to the uniform angular distribution on $[0;2\pi]$. ζ is obtained by numerically solving Eq. (28):

$$x_8 = \frac{\displaystyle\int_0^\zeta \int_0^\infty dn(p,q) p\, dp\, dq}{\displaystyle\int_0^\infty \int_0^\infty dn(p,q) p\, dp\, dq}$$

$$= \frac{\sin[2\arctan(\zeta/\zeta_0)] + 2\arctan(\zeta/\zeta_0)}{\pi} \qquad (28)$$

B. Transfer of the excitation energy

As for the infinitely long cylinder, the absorption-remission processes following the emission of photons from an initially excited state are counted until the photon reaches the walls. Three possibilities should then be considered for the real cell.

(i) The photon is absorbed by the inner walls: the emission being in the VUV domain. The stainless steel consti-
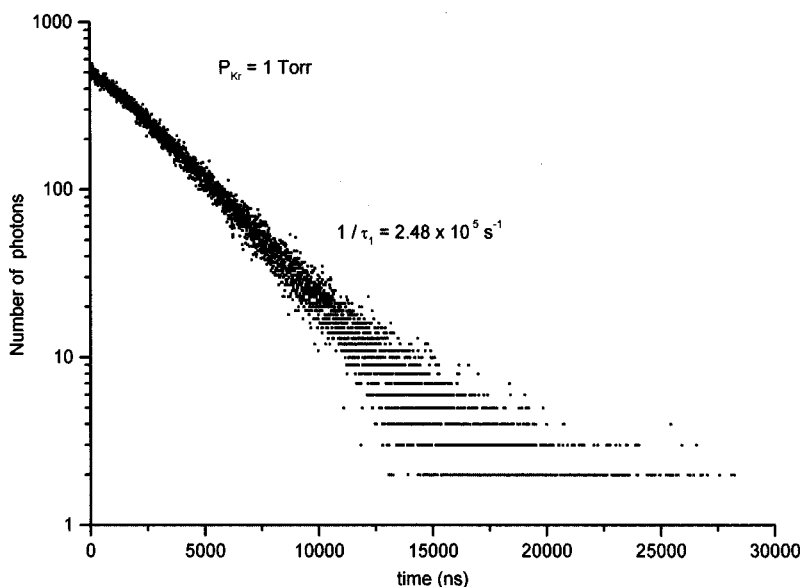
FIG. 6. Simulated temporal decay of the Kr($^3P_1$) emission in 1 Torr of pure krypton.

tutes an absorbent material for these photons.

(ii) The photon crosses the observation window without being detected by the photomultiplier tube.

(iii) The photon crosses the porthole and attains the photocathode. In this case, the characteristics of the photon are stored.

In all these cases, an excited state has disappeared from the cell. A new excited state created by the laser beam is then considered. This process is carried on until all the initially excited states are worked out.

C. Escape factor and the decay of luminescence with time

The escape factor is usually defined with regard to the overall photons leaving the vessel (Holstein [10], Payne and co-workers [7,11], Van Trigt [47], Molisch, Oehry and Margel [14], Lawler, Parker, and Hitchon [48]). However, as in any experimental apparatus, the detector is localized, and only the escape factor corresponding to the detected photons can be measured. In our experimental conditions, the escape factor thus determined is about 1.5 times smaller than the real one corresponding to photons reaching the walls. So in a real experiment, it depends on the size and position of the detector.

The mean number of absorption-remission processes allows the escape factor to be determined, but it can also be deduced from the temporal evolution of the number of photons using Eq. (1). The histogram (Fig. 6), obtained by classifying the detected photons according to their arrival time, provides the decay of the luminescence over time without any biased consideration for the law of variation of radiation trapping. In conformity with the fundamental mode of Holstein's theory, a single exponential term is sufficient to describe the decay of the luminescence on our time scale. The time constant τ_a is obtained by the maximum likelihood method used elsewhere for the experimental histograms. We verified that the ratio τ_a/τ_n determined in this way is close to the value of $1/g$ obtained from the mean number of

absorption-remission processes; the agreement is better than 1%.

D. Determination of the natural lifetime of the Kr($^3P_1$) resonant state

The natural lifetime $\tau_n = 3.97 \pm 0.18$ ns was deduced from the escape factor $g = (9.84 \pm 0.07) \times 10^{-4}$ obtained from the model and the experimentally determined apparent lifetime $\tau_a = 4.04 \pm 0.04 \, \mu$s. The value of the oscillator strength, calculated with Eq. (29), $f = 0.173 \pm 0.009$ is compared in Table I to other values found in the literature:

$$f = \frac{1}{\tau_n} \frac{mc}{8\pi^2} \frac{4\pi\varepsilon_0}{e^2} \frac{g_2}{g_1} \lambda_0^2. \qquad (29)$$

VI. EXPERIMENTAL STUDY OF THE KRYPTON-ARGON MIXTURE

A. Results

In order to study the influence of another rare gas on the trapping of resonance radiation in krypton, it is essential to be in conditions where no energy transfer takes place between the two gases. This is satisfied in the Kr-Ar mixture, since the first argon excited states are of higher energy than the Kr($^3P_1$) level.

For our purposes we have to seek conditions where luminescence essentially comes from either the resonance line or from the first continuum for which the resonant state is a precursor. This study was thus carried out for krypton pressures ranging from 1 to 6 Torr. The expression of the apparent lifetime depends only on the partial pressure ratio and so, on the concentration of the nonexcited gas [Eq. (15)]. In order to verify this property, we studied the Kr-Ar mixtures for different argon concentrations (90%, 98%, and 99%). Sufficiently high concentrations are used so as to observe a significant variation of the decay rate. For krypton pressures less than 4 Torr, a single exponential term suffices to de-
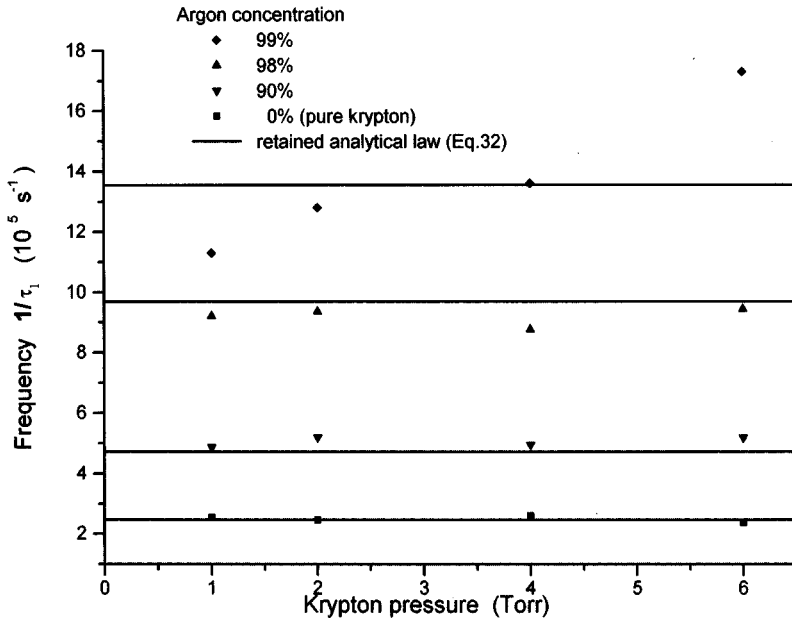
FIG. 7. Pressure dependence of the $Kr(^3P_1)$ decay frequency in Kr-Ar mixtures.

scribe the variation of the luminescence with time. This remains true at concentrations lower than 90%, as well as for krypton pressures between 4 and 6 Torr. For higher krypton pressures or argon concentrations, a second exponential term, of low amplitude, was considered. An experimental histogram obtained for 1 Torr of krypton at a concentration of 99% is shown in Fig. 4(b). The variation of the faster decay rate $1/\tau_1$ as a function of krypton pressure for constant argon concentrations is given by Figs. 7. The decay rate can be expressed as a function of the partial pressures:

$$\frac{1}{\tau_1} = \left(\alpha_1 + \alpha_2 \frac{P_{Ar}}{P_{Kr}} \right)^{1/2} + k_2 P_{Kr} + k_3 P_{Ar}$$
$$+ k_4 P_{Kr} P_{Ar} + k_5 P_{Kr}^2 + k_6 P_{Ar}^2. \tag{30}$$

At a constant argon concentration C, it is given by

$$\frac{1}{\tau} = \frac{1}{\tau_a} + \Gamma_1 P_{Kr} + \Gamma_2 P_{Kr}^2, \tag{31}$$

with

$$\frac{1}{\tau_a} = \left(\alpha_1 + \alpha_2 \frac{C}{1-C} \right)^{1/2}, \tag{32}$$

$$\Gamma_1 = k_2 + k_3 \frac{C}{1-C}, \tag{33}$$

and

$$\Gamma_2 = k_5 + k_4 \frac{C}{1-C} + k_6 \left(\frac{C}{1-C} \right)^2. \tag{34}$$

The data processing is performed in two steps. Firstly, in order to verify the compatibility of the experimental values with the theoretical formula, the parameters of Eq. (31) are estimated by a least-squares fit, for several constant concentrations, then $1/\tau_a^2$, Γ_1, and Γ_2 are drawn versus $C/(1-C)$. This first step indicates the collisional terms to be taken into account in the second step. Second, in the so-called global exploitation method, a definitive set of parameters from among α_1, α_2, k_2, k_3, k_4, k_5, and k_6, is estimated by a nonlinear least-squares method from the processed experimental points. For a given concentration, in the Kr-Ar mixture, the decay rate can be assumed to be constant over the whole krypton pressure range (Fig. 7), and the collision terms accounted for by both constants Γ_1 and Γ_2 can be discarded. The time constant is the apparent lifetime τ_a of the resonant state and $1/\tau_a^2$ varies linearly with $C/(1-C)$ (Fig. 8). The global method gave the values $\alpha_1 = (6.12 \pm 0.012) \times 10^{10} \, s^{-2}$ and $\alpha_2 = (1.79 \pm 0.05) \times 10^{10} \, s^{-2}$. Any other set of parameters led to negative or insignificant values of the collision rate constants.

B. Interpretation

The values of α_1 and α_2 allow the van der Waals broadening coefficient ξ_{Ar} to be determined if the value of the resonance broadening coefficient ξ_{Kr} is known (Sec. I B): $\xi_{Ar} = (\alpha_2/\alpha_1)\xi_{Kr}$. We can deduce the resonance broadening coefficient ξ_{Kr} from its theoretical expression (16) knowing the value of the oscillator strength of the transition $f = 0.173 \pm 0.009$. We find $\xi_{Kr} = 1.74 \times 10^{-15} \, m^3 \, s^{-1}$, and, for the van der Waals broadening coefficient $\xi_{Ar} = (5.10 \pm 0.24) \times 10^{-16} \, m^3 \, s^{-1}$, the broadening coefficient due to argon is smaller than the resonance coefficient as predicted by theory [16,18]. The results obtained confirm that the apparent lifetime remains constant for a given concentration. Figure 7 shows that its variation according to concentration cannot be ignored at high concentrations. For example, from pure gas to an argon concentration of 42% the decay rate varies by 10%; it reaches twice its value in the pure gas for a concentration of 90%. The decay of the $Kr(^3P_1)$ state through three-body collisions with two ground-state krypton
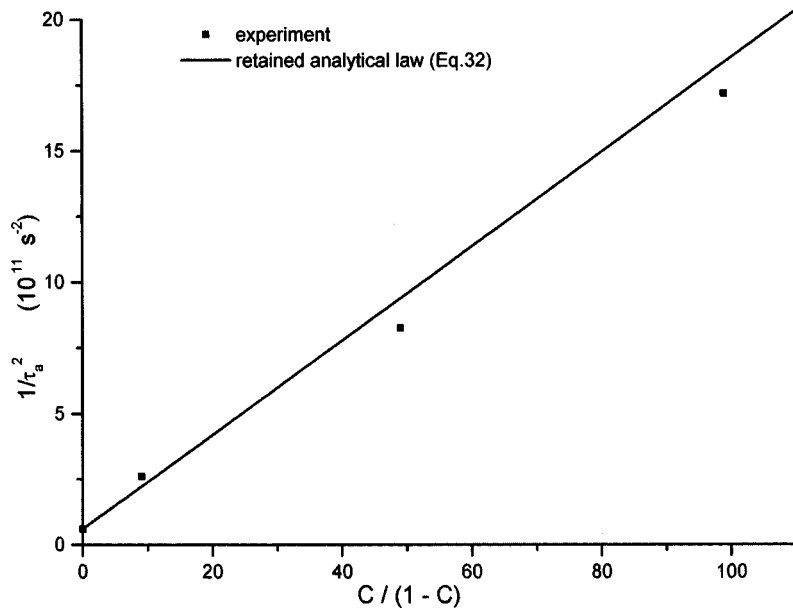
FIG. 8. Variation of $1/\tau_a^2$ as a function of ratio $C/(1-C)$ in Kr-Ar mixtures.

atoms can be ignored here: in mixtures where the krypton pressure never exceeds 6 Torr, the higher value of the decay term $116P_{Kr}^2$ (obtained in pure krypton), is always lower than the uncertainties on the decay rate. In such conditions, it does not seem possible to prove the existence of this term.

VII. EXPERIMENTAL RESULTS IN PURE XENON

The luminescence of the first resonance line and the first continuum of xenon were observed through an interferential filter centered at 145 nm and having a FWHM of 17.5 nm. The other experimental conditions were identical to those concerning the study of the first resonant state of krypton: the pressure domain ranged from 0.2 to 70 Torr and the time scale was 81 μs with a resolution of 5 ns.

As in krypton, when the pressure is less than 15 Torr, the luminescence decay is well described by a single exponential term. Figure 9 shows a parabolic variation of the correspond-

ing decay frequency $1/\tau_1$ with pressure, but it is quite constant from 0.2 to 6 Torr, as expected for pressure broadening when inelastic collisions can be ignored. Above 15 Torr, a second exponential term appears with a greater time constant τ_2.

A. Time constant τ_1

If we use the expression $1/\tau_1 = k_1 + k_2 P_{Xe} + k_5 P_{Xe}^2$, where the binary collisions are considered, the value of k_2 is negative and does not have any physical significance. The behavior of $1/\tau_1$ in xenon is similar to that in krypton.

$$\frac{1}{\tau_1} = k_1 + k_5 P_{Xe}^2, \tag{35}$$

with $k_1 = 1/\tau_a = (2.64 \pm 0.02) \times 10^{+5}$ s^{-1} and $k_5 = 218 \pm 11$ Torr^{-2} s^{-1}. This time constant can be attributed to the
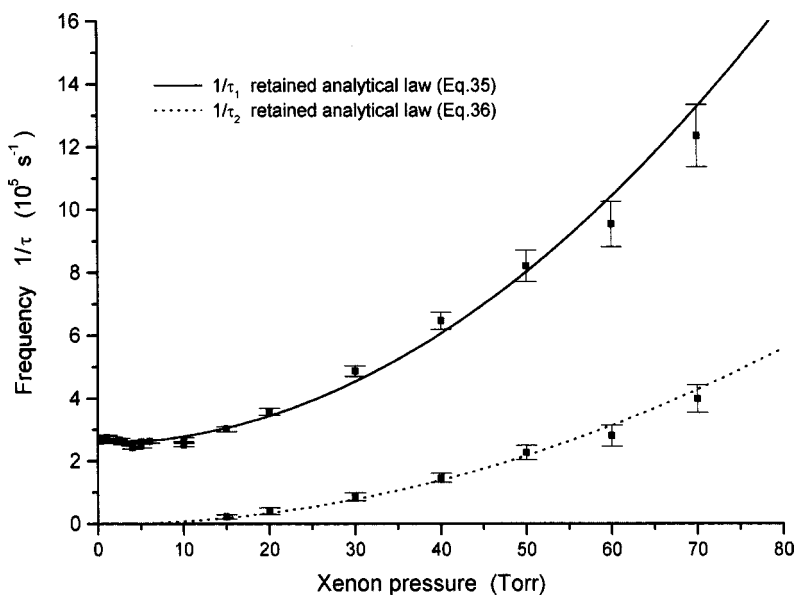

FIG. 9. Pressure dependence of the Xe($^3P_1$) and Xe($^3P_2$) decay frequencies in pure xenon.

TABLE VI. Two- and three-body rate constants relative to the decay of $Xe(^3P_1)$ in pure xenon.

k_2 (Torr^{-1} s^{-1})	k_5 (Torr^{-2} s^{-1})	Reference	k_2 (Torr^{-1} s^{-1})	k_5 (Torr^{-2} s^{-1})	Reference
	61	[75]		216	[76]
	99	[77]	9150	46	[43]
	161	[78]	700	150	[1]
	179	[79]	3350	27	[80]
				218±11	This work

$Xe(^3P_1)$ state, and the apparent lifetime is $\tau_a = 3.79 \pm 0.03 \ \mu s$. As in krypton, the natural lifetime $\tau_n = 3.98 \pm 0.18$ ns and the oscillator strength $f = 0.244 \pm 0.012$ were obtained after the determination of the escape factor $g = (1.052 \pm 0.07) \times 10^{-3}$ by our simulation program. The value of the oscillator strength is quite close to those reported in the literature (Table II). Constant k_5 expresses excimer formation:

$$Xe(^3P_1) + 2Xe(^1S_0)$$

$$\xrightarrow{k_5} Xe_2[0_u^+(^3P_1) \text{high } v] + Xe(^1S_0).$$
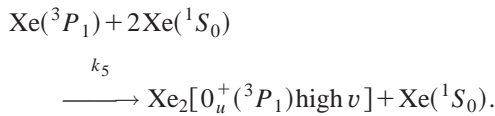
As in krypton, we were unable to measure the radiative lifetime of the $0_u^+(^3P_1)$ state since it is of the same order of magnitude as our resolution: Bonifield *et al.* [75], Haaks and Becker [76], and Keto *et al.* [74] gave lifetimes of 4.6 ± 0.3 ns, 5.7 ns, and 5.5 ns, respectively.

The two and three-body collision rate constants of the $Xe(^3P_1)$ state obtained by various authors are given in Table VI. Our result is in good agreement with the value found by Haaks and Becker [76], whose pressure domain is quite close to ours. Like us, they did not consider binary collision decay either. We again processed measurements done previously by Salamero *et al.* [1] on the same apparatus. The difference found for the values of k_2 and k_5 may come, as in pure krypton, from the recording and the processing of data which since, have been much improved.

Closer examination of Fig. 9 at low pressures reveals the presence of a very slight minimum at about 4 Torr. This phenomenon was observed before by Vermeersch *et al.* [8], [81] and Lange and Leipold [82]. This weak variation, not completely explained yet, is not taken into consideration in our variation law.

B. Time constant τ_2

As in krypton, the second exponential term appears only for pressures greater than 15 Torr. Its low amplitude leads to some uncertainties on the estimation of its time constant τ_2. However, in order to identify the precursor atomic state, we will present the results obtained, since the second exponential term was subjected to a complete survey in xenon-based mixtures, where this term appears over broader ranges of pressure. The general expression $1/\tau_2 = k_1' + k_2' P_{Xe} + k_5' P_{Xe}^2$ leads to values of k_1' and k_2' that bear uncertainties higher than 100%. Moreover, k_1' is negative. Discarding these two terms, our calculation leads to $k_5' = 87 \pm 5$ Torr^{-2} s^{-1}, with

$$\frac{1}{\tau_2} = k_5' P_{Xe}^2. \tag{36}$$

The absence of a constant term suggests an excited state with a long lifetime: the greatest value of τ_2, measured directly (44 μs), is much longer than the apparent lifetime of the resonant state. This time constant can therefore only be attributed to the $Xe(^3P_2)$ metastable state. Nonetheless, the presence of the latter does not question the selectivity of our excitation. The crossing of the potential curves of the $Xe_2[0_u^+(^3P_1)]$ state and the dissociative states 2_g, 2_u, 1_g, and 0_g^-, correlated to the $Xe(^3P_2)$, state should populate the metastable state during the vibrational relaxation on the 0_u^+ state. The $Xe(^3P_2)$ state then disappears by three-body collisions forming $Xe_2[1_u]$ (high v). The excimer can emit either from high vibrational levels in the spectral range of the first continuum, or after relaxation, in the second continuum with a maximum intensity at 170 nm. Considering the interferential filter's bandwidth and the pressure range, the emission observed probably comes rather from the higher vibrational levels. Moreover, we were not able to detect the well known lifetime of the lower levels (100 ns) which should be observable in our conditions if the emission comes from the lower vibrational levels. An emission at a shorter wavelength, from the higher levels having a smaller lifetime, is more likely. The determinations of k_5' by different authors (Table VII) are in very good agreement. This supports its attribution to the decay of $Xe(^3P_2)$.

TABLE VII. Three-body rate constants relative to the decay of $Xe(^3P_2)$ in pure xenon.

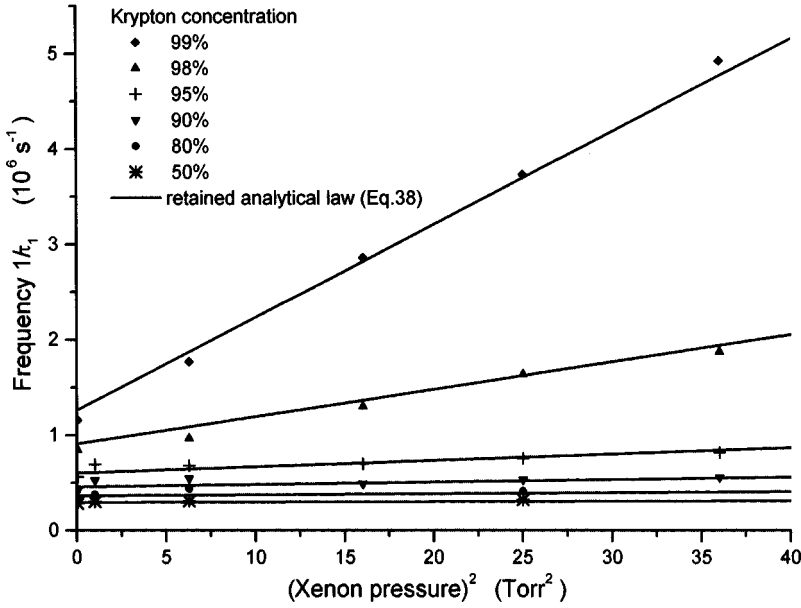| k_5' (Torr^{-2} s^{-1})	Reference	k_5' (Torr^{-2} s^{-1})	Reference	k_5' (Torr^{-2} s^{-1})	Reference
85	[1]	82	[83]	61	[86]
92	[68]	87	[84]	81	[87]
85	[78]	89	[85]	87±5	This work

FIG. 10. Variation of the Xe($^3P_1$) decay frequency as a function of P_{Xe}^2 in Xe-Kr mixtures.

VIII. EXPERIMENTAL STUDY OF THE XENON-KRYPTON MIXTURE

A. Results

The study of the Xe-Kr mixtures was performed in the same excitation and detection conditions as for pure xenon. We measured the decay of the luminescence for six krypton concentrations ranging from 50% to 99%, and for xenon pressures varying from 0.2 to 20 Torr. As in pure xenon, the time constant τ_1, can be observed over the whole pressure range. The second exponential term can be determined only for pressures higher than 15 Torr in the pure gas, and at xenon partial pressures which decrease as the krypton concentration increases [88].

1. Time constant τ_1

The variation of the decay rate $1/\tau_1$ versus xenon pressure is presented in Fig. 10 for the different constant krypton concentrations. At high concentrations, the contribution of the inelastic collisions is clear. The general expression of the time constants is similar to that of Eq. (31):

$$\frac{1}{\tau_1} = \frac{1}{\tau_a} + \Gamma_1 P_{\text{Xe}} + \Gamma_2 P_{\text{Xe}}^2. \tag{37}$$

The way the data were processed was already discussed in Sec. VI A: first of all, τ_a, Γ_1, and Γ_2 were estimated for each concentration, so as to assess the involvement of two and three-body collision terms and, for the apparent lifetime, to allow verification of the agreement with relation (32). For every concentration, the linear variation of $1/\tau_1$ as a function of the square of the xenon pressure (Fig. 10) shows that the term Γ_1, corresponding to binary collisions, is negligible. In Fig. 11(b) the square of the different y intercepts of Fig. 10 is given as a function of $C/(1-C)$. This shows that $1/\tau_a$ is in good agreement with its theoretical expression. Similarly, the three-body collision terms can be evaluated by plotting the variation of the slopes of the straight lines (i.e., Γ_2) of Fig.

10 versus $C/(1-C)$. If we refer to Eq. (34), its parabolic variation [Fig. 11(a)] indicates that the three terms k_4, k_5, k_6 are present:

$$\frac{1}{\tau_1} = \left(\alpha_1 + \alpha_2 \frac{C}{1-C} \right)^{1/2} + k_4 P_{\text{Xe}} P_{\text{Kr}} + k_5 P_{\text{Xe}}^2 + k_6 P_{\text{Kr}}^2. \tag{38}$$

As before, the constants of Eq. (38) were obtained by global processing of the overall experimental data set corresponding to the pure gas as well as the mixture. The values for the apparent lifetime are $\alpha_1 = (6.98 \pm 0.11) \times 10^{10}$ s^{-2} and $\alpha_2 = (1.55 \pm 0.06) \times 10^{10}$ s^{-2}, while, for the collision terms, $k_4 = 187 \pm 14$ Torr^{-2} s^{-1}, $k_5 = 215 \pm 12$ Torr^{-2} s^{-1}, and $k_6 = 7.94 \pm 0.24$ Torr^{-2} s^{-1}

2. Time constant τ_2

The time constant τ_2 which only appears at high partial pressures (50% of our measurements) was assigned, in the pure gas, to the metastable state. The collision terms can be found by plotting the decay frequency where either a partial pressure or the concentration is kept constant (Fig. 12). The variation law can thus be deduced:

$$\frac{1}{\tau_2} = k_1' + k_3' P_{\text{Kr}} + k_4' P_{\text{Xe}} P_{\text{Kr}} + k_5' P_{\text{Xe}}^2. \tag{39}$$

Again, the reaction constants are determined by the global data processing approach: $k_1' = (2.04 \pm 0.33) \times 10^4$ s^{-1}, $k_3' = 131 \pm 20$ Torr^{-1} s^{-1}, $k_4' = 44 \pm 2$ Torr^{-2} s^{-1}, and $k_5' = 85 \pm 6$ Torr^{-2} s^{-1}.

Among the decay frequencies measured for $P_{\text{Xe}} = 20$ Torr, there are six values which deviate from those deduced from the final estimates of the rate constants [the solid line of Fig. 12(b)]. This reveals the less good quality of the estimation of τ_2, owing to the low amplitude of the corresponding exponential term.
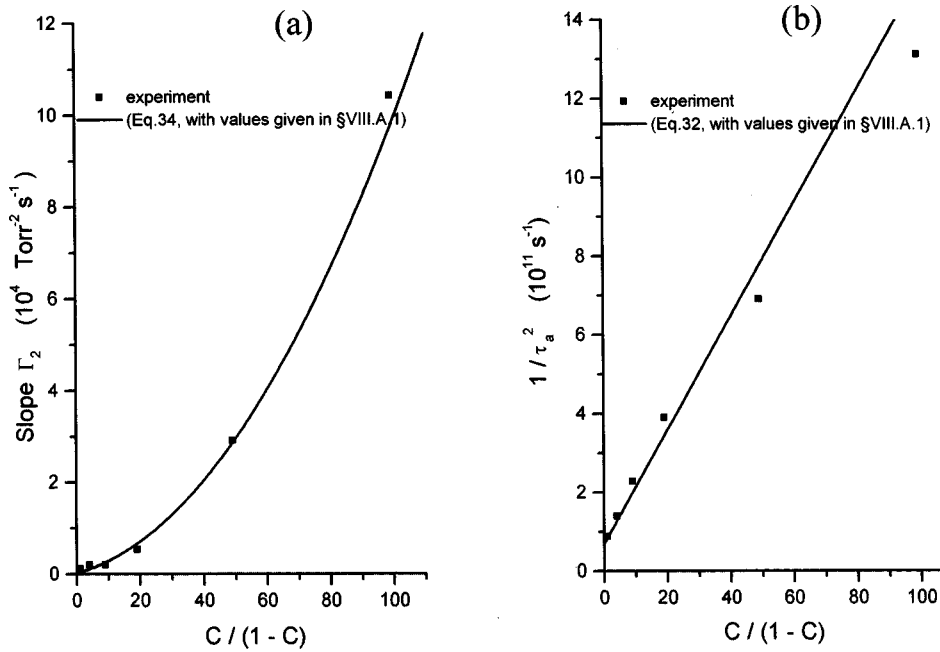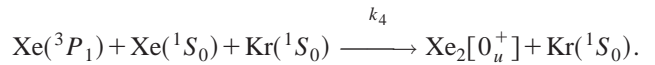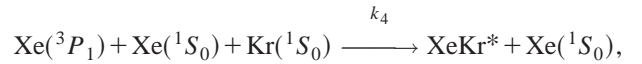
FIG. 11. Variation of the slope Γ_2 (a) and $1/\tau_a^2$ (b), deduced from Fig. 10, vs $C/(1-C)$ in Xe-Kr mixtures.

B. Interpretation

1. Decay of the $Xe(^3P_1)$ state

The van der Waals broadening coefficient ξ_{Kr} can be deduced from the two coefficients α_1 and α_2, because the resonance broadening coefficient $\xi_{Xe}=2.92\times10^{-15}$ m^3 s^{-1} can be calculated from its theoretical expression (16) with $f=0.244\pm0.012$. The main difference with the value $\xi_{Xe}=2.03\times10^{-15}$ m^3 s^{-1}, suggested by Igarashi *et al.* [12], comes from their choice of the resonance interaction constant K [89], which has since been subjected to an erratum correction [49]. Our determination of the broadening coefficient due to krypton $\xi_{Kr}=(\alpha_2/\alpha_1)\xi_{Xe}=(6.48\pm0.33)\times10^{-16}$ m^3 s^{-1} is lower than that due to resonance as predicted by theory.

The absence of two-body collisions confirms that there is no energy transfer between the two gases. Constant k_4 corresponds to reactions

$$Xe(^3P_1)+Xe(^1S_0)+Kr(^1S_0) \xrightarrow{k_4} XeKr^*+Xe(^1S_0),$$

$$Xe(^3P_1)+Xe(^1S_0)+Kr(^1S_0) \xrightarrow{k_4} Xe_2[0_u^+]+Kr(^1S_0).$$

Its value $k_4=187\pm14$ Torr^{-2} s^{-1} is just slightly lower than the homonuclear collision rate constant k_5 associated to the formation of excimer $Xe_2[0_u^+]$. The value of k_5 is very close to that obtained in the pure gas. k_6 can represent the collision process
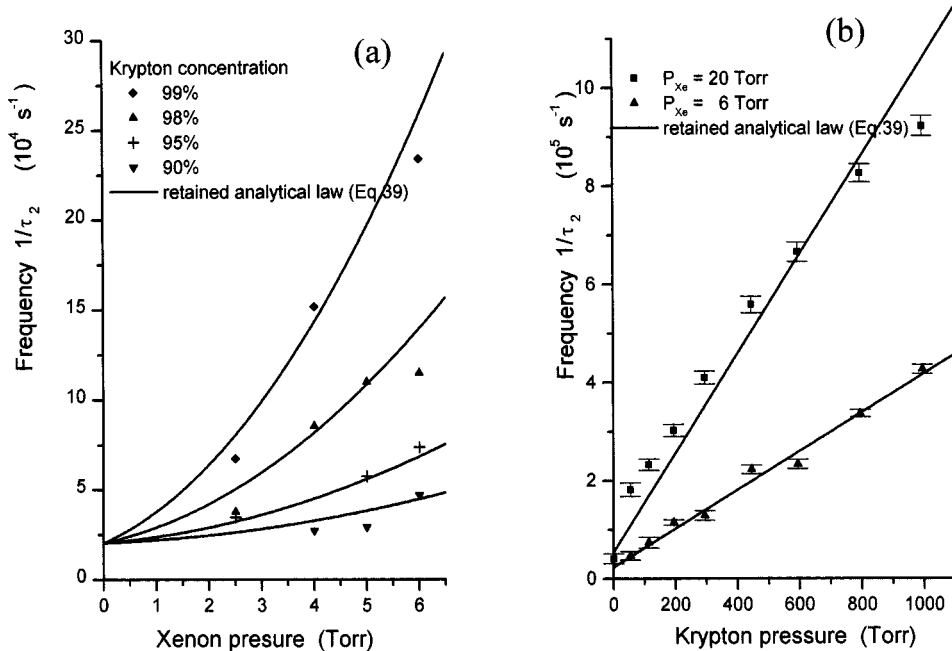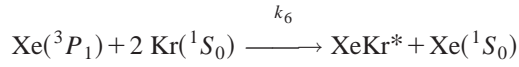

FIG. 12. Variation of the $Xe(^3P_2)$ decay frequency with P_{Xe} (a) and P_{Kr} (b) in Xe-Kr mixtures.

$$\text{Xe}(^3P_1) + 2\text{ Kr}(^1S_0) \xrightarrow{k_6} \text{XeKr*} + \text{Xe}(^1S_0)$$

with the creation of the excimer XeKr*. This molecule would emit within the xenon first continuum. Below *et al.* [90] demonstrated an emission of this molecule at 156.5 nm.

An emission centered at 163 nm, with a much greater spectral width (28 nm) than that due to the xenon or krypton excimers, was observed by Kubodera *et al.* [91] in Xe-Kr mixtures. A contribution of the XeKr* excimer was suggested by the authors.
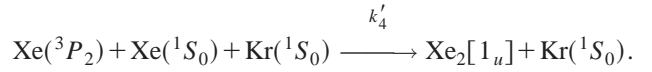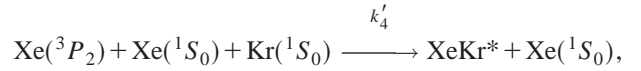
Montagné [45] undertook a study of this binary mixture, excited by α particles. At 173 nm, he attributed a time constant to the Xe($^3P_1$) state following: $1/\tau = 45P_{\text{Xe}}P_{\text{Kr}}$, which corresponds to heteronuclear collisions. However, from their own results, Berejny [92] and Marchal [36] showed that an attribution to the Xe($^3P_2$) state would be more suitable. Our results also support this.

Cook and Leichner [93], on the same mixture excited by an electron beam, suggested extensive involvement of binary collisions for the Xe($^3P_1$) state, leading to the creation of the Xe($^3P_2$) metastable state: $1/\tau = \beta_0 + 10^4 P_{\text{Xe}} + 2100P_{\text{Kr}} + 97P_{\text{Kr}}P_{\text{Xe}} + 7P_{\text{Kr}}^2$. However, considering their pressure range (the xenon pressure can reach 90 Torr), the absence of a term corresponding to P_{Xe}^2 is in contradiction with our results in pure xenon. Moreover, these authors did not account for the van der Waals broadening by krypton. On the other hand, agreement is excellent for k_6.

2. Decay of the Xe($^3P_2$) state

As in pure xenon (Sec. VII B), the excimer molecules Xe$_2$[0_u^+] lead to the creation of the Xe($^3P_2$) state through vibrational relaxation and the crossing of the dissociative potential curves. However the time constant τ_2 associated to the metastable state appears at lower xenon pressures in the mixtures. This results from the excimer formation by three-body heteronuclear collisions which favor the creation of the metastable state. In addition, vibrational relaxation of the Xe$_2$[0_u^+($^3P_1$)] (high v) state must be supported by heteronuclear collisions.

The constant term k_1' leads to an apparent lifetime of 49 μs, greater than any known lifetime, and which can only be assigned to the Xe($^3P_2$) state. For the collision rate constant $k_3' = 131 \pm 20$ Torr^{-1} s^{-1}, the reaction products have not been satisfactorily identified since the populating of the resonant state by binary collisions should also be accompanied by an inverse reaction from this state. Some inaccuracy in our results can also be considered, since the determination of this second exponential term is rather difficult. Nevertheless, our results are in good agreement with those obtained by Marchal [36], who studied the energy transfer from krypton to xenon, and where the Xe($^3P_2$) state is created through cascades from a 5d state. He suggested the variation law $1/\tau = 120P_{\text{Kr}} + 38.7P_{\text{Kr}}P_{\text{Xe}}$. Considering the concentrations he used, the term representing the decay of this state by three-body homonuclear collisions is negligible. Constant k_4' corresponds to reactions

$$\text{Xe}(^3P_2) + \text{Xe}(^1S_0) + \text{Kr}(^1S_0) \xrightarrow{k_4'} \text{XeKr*} + \text{Xe}(^1S_0),$$

$$\text{Xe}(^3P_2) + \text{Xe}(^1S_0) + \text{Kr}(^1S_0) \xrightarrow{k_4'} \text{Xe}_2[1_u] + \text{Kr}(^1S_0).$$

Our determination is close to the result of Marchal, and coincides with that obtained by Montagne [45], assigned to the $^3P_1$ state by the latter. The homonuclear three-body collision rate constant k_5' is equal to 85 ± 6 Torr^{-2} s^{-1}, and is in good agreement with our results in pure xenon.

IX. EXPERIMENTAL STUDY OF THE XENON-ARGON MIXTURE

A. Variation of $1/\tau_1$

In the Xe-Ar mixtures, the experimental conditions were unchanged, and the behaviors of the time constants τ_1 and τ_2 with respect to the partial pressures were similar to that observed in Xe-Kr mixtures. The variation of $1/\tau_1$ with xenon pressure (Fig. 13), for a given concentration, should be attributed to the decay of the resonant state by collision. As in the previous studies, the variation law of the decay frequency versus the partial pressures was first established separately for each concentration (Fig. 14). The linear variation of $1/\tau_1$ with P_{Xe}^2 (Fig. 13) shows that the linear term Γ_1 of $1/\tau = (1/\tau_a) + \Gamma_1 P_{\text{Xe}} + \Gamma_2 P_{\text{Xe}}^2$ can be ignored, and the variation of Γ_2 versus $C/(1-C)$ [Fig. 14(b)] shows that only the two three-body collision terms k_4 and k_5 are significant whereas k_6 is negligible. The estimation of the y intercepts of Fig. 13 permits the verification of the linear variation of $1/\tau_a^2$ versus $C/(1-C)$, in conformity with theory [Fig. 14(a)]. The actual collisional and radiative rate constants were evaluated in a second step by processing the entire set of data with the retained expression

$$\frac{1}{\tau_1} = \left(\alpha_1 + \alpha_2 \frac{C}{1-C}\right)^{1/2} + k_4 P_{\text{Xe}}P_{\text{Ar}} + k_5 P_{\text{Xe}}^2, \quad (40)$$

with $\alpha_1 = (7.04 \pm 0.07) \times 10^{10}$ s^{-2}, $\alpha_2 = (9.07 \pm 0.25) \times 10^9$ s^{-2}, $k_4 = 93 \pm 4$ Torr^{-2} s^{-1}, and $k_5 = 225 \pm 13$ Torr^{-2} s^{-1}.

B. Variation of $1/\tau_2$

Figure 15 illustrates the variation of the decay frequency $1/\tau_2$ with xenon pressure. Figure 15(b) shows that at a given xenon pressure it varies linearly with argon pressure. The expression finally retained after a global approach is

$$\frac{1}{\tau_2} = k_3' P_{\text{Ar}} + k_4' P_{\text{Ar}}P_{\text{Xe}} + k_5' P_{\text{Xe}}^2, \quad (41)$$

with $k_3' = 162 \pm 23$ Torr^{-1} s^{-1}, $k_4' = 24 \pm 3$ Torr^{-2} s^{-1}, and $k_5' = 91 \pm 6$ Torr^{-2} s^{-1}.
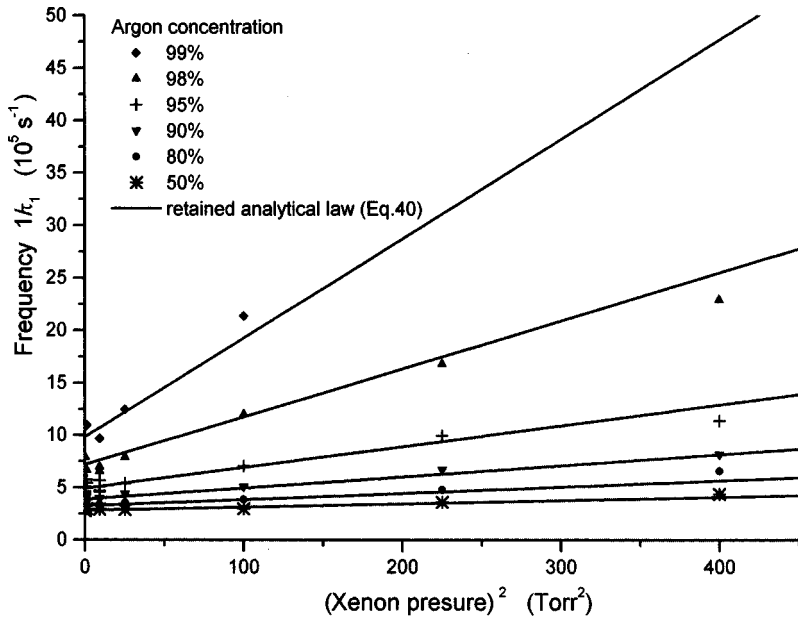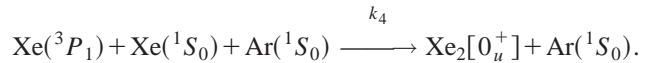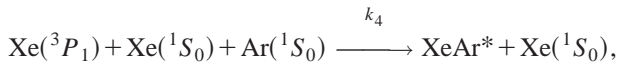
FIG. 13. Variation of the Xe($^3P_1$) decay frequency as a function of P_{Xe}^2 in Xe-Ar mixtures.

C. Interpretation

1. Resonant state

The broadening coefficient of the xenon resonance line due to argon is about eight times smaller than the resonance broadening coefficient: $\xi_{Ar} = (\alpha_2/\alpha_1)\xi_{Xe} = (3.76 \pm 0.16) \times 10^{-16}$ m^3 s^{-1}. Constant α_1 is independent of the added gas, as expected; close values are obtained in the xenon-krypton $(6.98 \pm 0.11) \times 10^{10}$ s^{-2} and the Xe-Ar $(7.04 \pm 0.07) \times 10^{10}$ s^{-2} mixtures.

The reactions

$$\text{Xe}(^3P_1) + \text{Xe}(^1S_0) + \text{Ar}(^1S_0) \xrightarrow{k_4} \text{XeAr*} + \text{Xe}(^1S_0),$$

$$\text{Xe}(^3P_1) + \text{Xe}(^1S_0) + \text{Ar}(^1S_0) \xrightarrow{k_4} \text{Xe}_2[0_u^+] + \text{Ar}(^1S_0).$$

correspond to a constant k_4. The rate constant k_5 corresponds to 0_u^+ excimer formation by three-body homonuclear collisions. Its determinations for three independent situations, namely, in the pure gas and in the two xenon based mixtures, are compatible. No two-body collision decay of the Xe($^3P_1$) state is observed, as suggested by the absence of any coincidence of argon and xenon energy levels.

Our works can be compared (Table VIII) to those of Gleason *et al.* [94] and Brunet *et al.* [58], for similar pressures and wavelengths. In addition to the three-body heteronuclear reaction previously described, these authors also considered
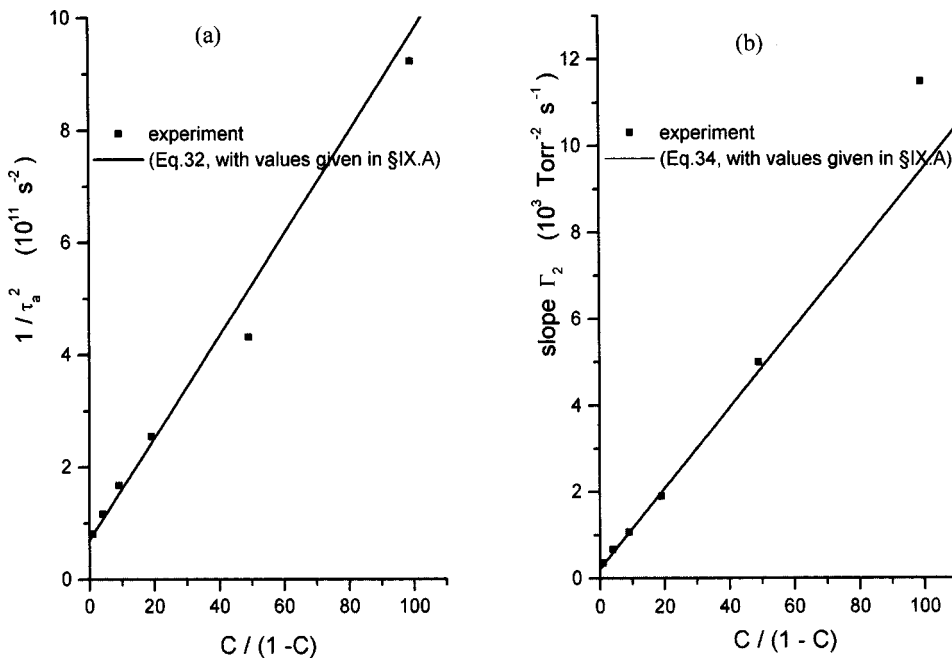

FIG. 14. Variation of the slope Γ_2 (a) and $1/\tau_a^2$ (b), deduced from Fig. 13, vs $C/(1-C)$ in Xe-Ar mixtures.
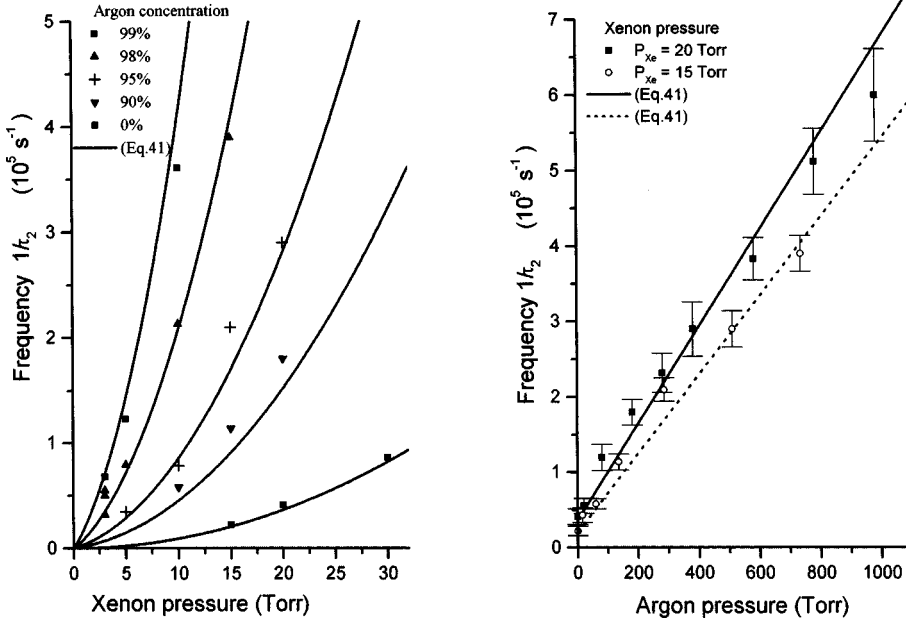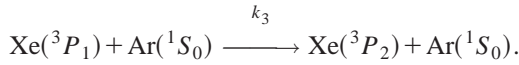
FIG. 15. Variation of the Xe($^3P_2$) decay frequency with P_{Xe} (a) and P_{Ar} (b) in Xe-Ar mixtures.

decay of the resonant state by binary heteronuclear collision

$$\mathrm{Xe}(^3P_1)+\mathrm{Ar}(^1S_0) \xrightarrow{k_3} \mathrm{Xe}(^3P_2)+\mathrm{Ar}(^1S_0).$$

The discrepancies are not at all surprising if, with hindsight, we closely examine the interpretations of the results put forward by in Refs. [94] and [58]. In Gleason *et al.*'s experiment, the energy transfer towards xenon populates the Xe($^3P_1$) state by cascades. According to these authors, the decay frequency follows $1/\tau_1 = k_3 P_{Ar} + k_4 P_{Xe} P_{Ar}$. But the apparent lifetime is not constant since argon is in a considerable majority in the mixture: the argon concentration varies and exceeds 99%. Let us plot, like Gleason *et al.* $1/\tau_1 P_{Ar}$ against xenon pressure, for high argon pressures and low xenon pressures; Eq. (40) gives $1/\tau_1 P_{Ar} \approx \sqrt{\alpha_2/P_{Ar} P_{Xe}} + k_4 P_{Xe}$. The linear variation at the higher xenon pressures corresponds to three-body heteronuclear collision reactions, in agreement with our results. But for low xenon pressures, the variation is no longer linear for a constant argon pressure, and we may have doubts about the interpretation considering a binary collision term.

In the kinetic study of this mixture by Brunet *et al.* at 145 nm, Xe($^3P_1$) is created by energy transfer from argon to xenon. The pressure ranges from 0.2 to 6 Torr for xenon and from 300 to 800 Torr for argon. One time constant is attributed to the decay of the first xenon resonant state and its expression is as follows: $1/\tau_1 = k_1 + k_3 P_{Ar} + k_4 P_{Xe} P_{Ar}$.

Brunet *et al.'s* results disagree with ours: for instance, in a set of measurements where argon pressure remains constant ($P_{Ar}=400$ Torr), while xenon pressure varies from 0.2–3.6 Torr, the time constant measured by Brunet *et al.* varies very little. However, $C/(1-C)$ increases by a factor of 18, and a variation of the apparent lifetime should have been observed. Neither Gleason *et al.* nor Geiger ever considered three-body collisions with two ground state-argon atoms. This is in contradiction with our results since at such sufficiently high pressures, Geiger's or Gleason *et al.*'s results should have brought its presence to the fore.

2. Metastable state

As in the Xe-Kr mixture, the second time constant appears for lower xenon pressures compared to the pure gas, because of heteronuclear collisions which contribute to the excimer formation. In the expression retained for the variation law of $1/\tau_2$ [Eq. (41)], the absence of a constant term confirms that it can only be attributed to the Xe($^3P_2$) metastable state.

The constant k_5' is associated with

$$\mathrm{Xe}(^3P_2)+2\mathrm{Xe}(^1S_0) \xrightarrow{k_5'} \mathrm{Xe}_2[1_u(^3P_2)]+\mathrm{Xe}(^1S_0).$$
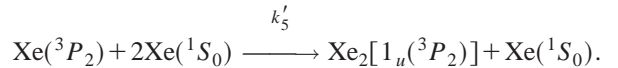
The agreement between the values found in the pure xenon 87 ± 5 Torr^{-2} s^{-1} and in Xe-Ar mixtures 91 ± 6 Torr^{-2} s^{-1} is satisfactory. The two- and three-body collision rate constants obtained by various authors are given in Table IX.

The following reactions can be associated with the rate constant k_4':

TABLE VIII. Two- and three-body rate constants for the decay of Xe($^3P_1$) in Xe-Ar mixtures.

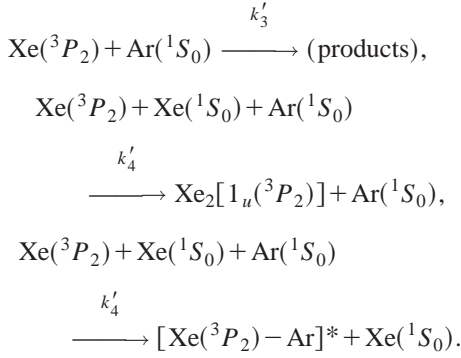| k_3 (Torr^{-1} s^{-1})	980	494 ± 99	
k_4 (Torr^{-2} s^{-1})	51	228 ± 22	93 ± 4
Reference	[58]	[94]	This work

TABLE IX. Two- and three-body rate constants for the decay of Xe($^3P_2$) in Xe-Ar mixtures.

k_3' (Torr^{-1} s^{-1})	6	11 ± 2		162 ± 23
k_4' (Torr^{-2} s^{-1})	28	27 ± 3	29	24 ± 3
Reference	[58]	[94]	[95]	This work

$$\text{Xe}(^3P_2) + \text{Ar}(^1S_0) \xrightarrow{k_3'} (\text{products}),$$

$$\text{Xe}(^3P_2) + \text{Xe}(^1S_0) + \text{Ar}(^1S_0)$$

$$\xrightarrow{k_4'} \text{Xe}_2[1_u(^3P_2)] + \text{Ar}(^1S_0),$$

$$\text{Xe}(^3P_2) + \text{Xe}(^1S_0) + \text{Ar}(^1S_0)$$

$$\xrightarrow{k_4'} [\text{Xe}(^3P_2) - \text{Ar}]^* + \text{Xe}(^1S_0).$$

The different values associated to the decay of the $\text{Xe}(^3P_2)$ state by three-body heteronuclear collisions are in very good agreement. This reaction should allow the formation of a Xe-Ar excimer. However, the dissociation of these excited states should be very fast because of their low bond energies. Gleason *et al.* [94] and Brunet *et al.* [58] only associated this collision rate constant with the formation of the $\text{Xe}_2(1_u)$ excimer. According to these authors, the constant corresponding to binary collisions k_3' expresses the decay of the $\text{Xe}(^3P_2)$ state in creating

$$\text{Xe}(^3P_1): \text{Xe}(^3P_2) + \text{Ar}(^1S_0) \xrightarrow{k_3'} \text{Xe}(^3P_1) + \text{Ar}(^1S_0).$$
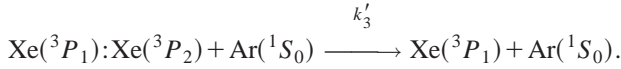
But, the inverse reaction should also occur. Gleason *et al.* put forward another interpretation considering the decay of the metastable state by induced collisions:

$$\text{Xe}(^3P_2) + \text{Ar}(^1S_0) \rightarrow \text{Xe}(^1S_0) + \text{Ar}(^1S_0) + h\nu$$

$$(\lambda \approx 147 \text{ nm}).$$
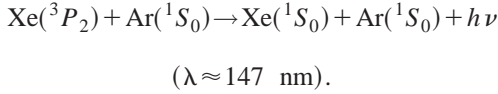
X. MODELING OF RADIATION TRAPPING IN BINARY MIXTURES

The final aim of this model was to calculate the escape factor **g** in most geometrical and pressure conditions. Especially in binary mixtures both the resonance and the experimentally determined van der Waals broadening coefficients can be introduced as initial data. In order to account for the decay of the resonant state by inelastic collision, we defined the collisional decay probability.

This program also gives certain information which we can attain with difficulty by experiment, such as for example, the spectral distribution of the photons detected, the dependence of the escape factor on certain physical parameters of either the excitation or the photon detection device.

A. Radiative and collisional decay of the resonant states

An isolated atom can decay radiatively with the probability

$$P_{\text{rad}} = \frac{1/\tau_n}{(1/\tau_n) + F_c} \tag{42}$$

in the presence of collisions of frequency: $F_c = k_2 P_x + k_3 P_y + k_4 P_x P_y + k_5 P_x^2 + k_6 P_y^2$. The collisions are thus introduced

in our calculations, using a random number x_{10} uniformly distributed over [0;1]. A photon is emitted only if $0 \leqslant x_{10} \leqslant P_{\text{rad}}$. If not, the resonant state disappears by collision, the calculation is given up, and a new initially created resonant state is considered. The introduction of the collisions in the elementary processes does not presuppose anything about the decay law of the density of the excited states. An alternative consists in adding the radiative decay frequency to that of collisional decay, for a single exponential decay law: when collisions occur, the exponential solution of Eq. (2): $n(\vec{r},t) = m(\vec{r})\exp(-\beta t)$, with $\beta = (g/\tau_n) + F_c$, leads to the escape factor defined previously: $g = 1 - [1/m(\vec{r})]\int_{\text{volume}} m(\vec{r}')G(\vec{r},\vec{r}')dv'$.

B. Study of the first xenon resonance line in xenon-krypton mixtures

The calculations are performed in the same conditions as in pure gas (Sec. V). Furthermore, for the mixtures, we introduce the measured van der Waals broadening coefficient and the collision rate constants. For example, here we give some results obtained by simulation for the Xe-Kr mixture for xenon pressures ranging from 1 to 6 Torr, and for krypton concentrations between 50% and 99%. In Fig. 16, the decay frequency of the resonant state is plotted versus xenon partial pressure for different krypton concentrations. The values obtained from the simulation program were compared to the experimental ones. The agreement is quite good and the relative difference always less than 5%.

C. Evidence of self-absorption

In our conditions of low light flux, recording the emission spectra of the resonance line with satisfactory resolution is impossible. On the other hand, this is possible with our model, by classifying the photons detected according to their wavelength. The spectra (Fig. 17) concern the Kr-Ar mixture with a complete frequency redistribution. The ordinate represents the density of the probability of obtaining a photon of frequency ν. Each spectrum presents the characteristic shape of the autoabsorption phenomenon. Examination of this figure shows that: (1) the maximum value of the probability density, occurring at ν_{max}, decreases as the concentration increases; (2) the interval $(\nu_{\text{max}} - \nu_0)$ increases with argon concentration; (3) as the concentration increases, the presence of photons coming from the wings is favored and such photons have less chance of being trapped. Therefore, the apparent lifetime decreases when the concentration of the foreign gas increases.

XI. CONCLUSION

The van der Waals broadening coefficients ξ_Y of the first resonance line of krypton and xenon, due to a lighter rare gas, have been determined in conditions where the variation of the apparent lifetime is easily observed:

(i) Our method of selective excitation of the resonant states allows us to work with concentrations of the added gas higher than 50%, without excitation of the latter.
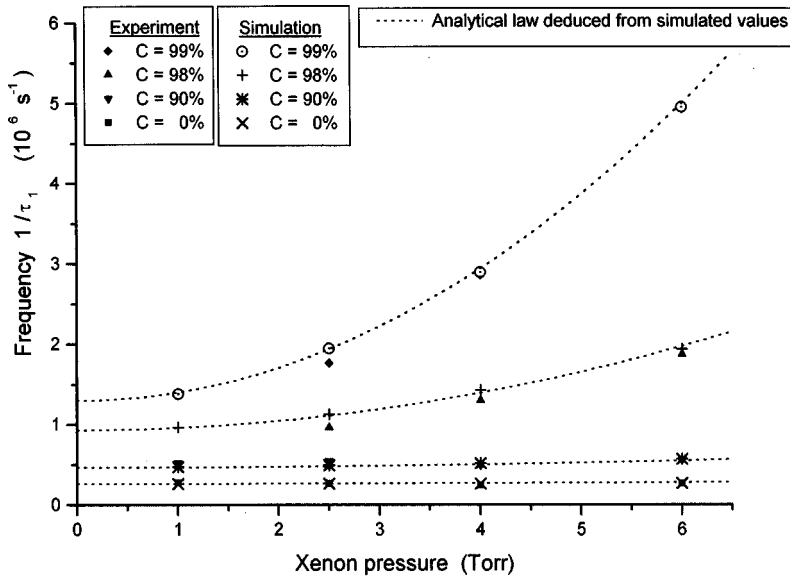
(ii) The very efficient transfers between rare gases are

FIG. 16. Comparison of the simulated Xe($^3P_1$) decay frequency with experimental results in Xe-Kr mixtures.

avoided by using lighter added gases.

(iii) The pressure of the excited gas is sufficiently low for the three-body homonuclear reaction to be unlikely. It is, however, sufficiently high to assume pressure broadening and complete frequency redistribution.

The coupling of the apparent lifetime measurements with the modelling of resonance radiation trapping in our real experimental conditions proves to be a powerful tool. The determination of the oscillator strength of the transition, associated with the measurement of the apparent lifetime in mixtures gives the van der Waals broadening coefficients for the added gases. Simultaneously, three-body heteronuclear reaction rates for resonant states are measured. A careful calculation of the precision of the measured constants greatly facilitated the discussion about the reactions that should be accounted for. Henceforth, the introduction of the overall results in our program of modeling will allow us to calculate the decay frequency of resonant states in any conditions.

Currently, we are carrying on with these works by studying the influence of neon and helium on these resonant lines. A comparison with Igarashi's work [12] concerning the xenon resonance line at 146.96 nm will then be possible. Our experimental device may also allow us to selectively excite the Xe($^1P_1$) resonant state. The study of the influence of lighter rare gases on the second resonance line of xenon at 129.6 nm could thus be achieved. These are our main short-term objectives.

APPENDIX

In an infinitely long cylinder, resonance radiation trapping for an optically thick medium where pressure broadening is predominant leads to an apparent lifetime τ_a proportional to $\sqrt{k_p(\nu_0)}$ [where $k_p(\nu_0)$ is the absorption coefficient at the central wavelength of the resonance line]. As established in
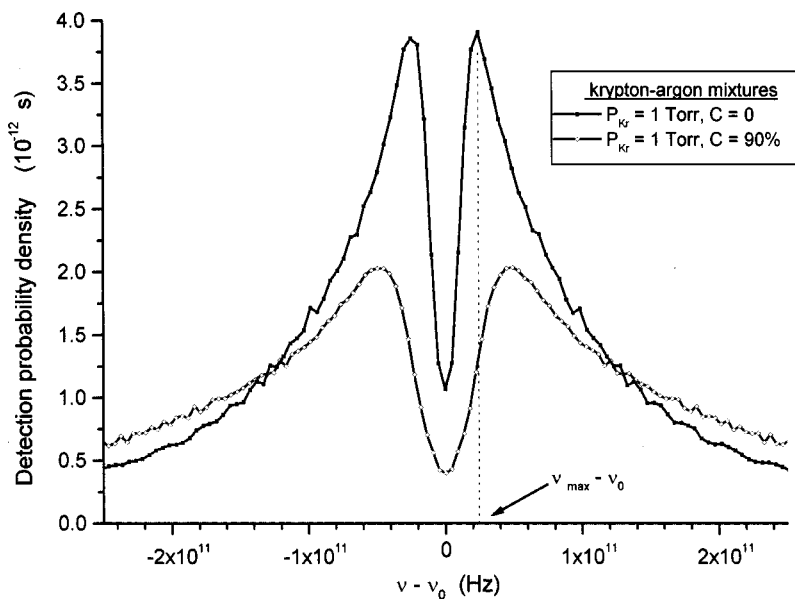

FIG. 17. Simulated spectra of the krypton resonance line in pure krypton and Kr-Ar mixtures.

Eq. (13) in Sec. I B for a binary mixture X-Y in the same conditions, τ_a is proportional to $\sqrt{k_T(\nu_0)}$, and depends on ξ_X and ξ_Y, the resonance broadening coefficient and the van der Waals broadening coefficient, respectively, and on the densities of the ground state of atoms X and Y, N_{0X} and N_{0Y},

respectively.

For a more complex geometry, the same dependence of τ_a on the densities N_{0X} and N_{0Y} can be expected, if we consider the expression of the escape factor as a function of the resonant state density $n(\vec{r})$, established by Holstein [9,10]:

$$g = \frac{\int_{\text{cell volume}} n^2(\vec{r})E(\vec{r})dv + \frac{1}{2}\int_{\text{cell volume}}\int [n(\vec{r})-n(\vec{r}')]^2 G(\vec{r},\vec{r}')dv\,dv'}{\int_{\text{cell volume}} n^2(\vec{r})dv}.$$

Since $G(\vec{r}',\vec{r})$ is proportional to $1/\sqrt{k_T(\nu_0)}$ [10], we can write $G(\vec{r}',\vec{r})=[1/\sqrt{k_T(\nu_0)}]f(\vec{r}',\vec{r})$. For $E(\vec{r})$, Holstein pointed out that it can be obtained by the integration over the volume external to the cell and filled with the absorbing gas since the integral of $G(\vec{r}',\vec{r})$ over an infinite volume is equal to 1: $E(\vec{r})=1-\int_{\text{cell volume}}G(\vec{r},\vec{r}')dv'=\int_{\text{ext. volume}}G(\vec{r},\vec{r}')dv'$.
Then $E(\vec{r})$ is also proportional to $1/\sqrt{k_T(\nu_0)}$, and so for the escape factor g:

$$g = \frac{1}{\sqrt{k_T(\nu_0)}}\frac{\int_{\text{cell volume}} n^2\left(\vec{r}\int_{\text{ext. volume}} f(\vec{r},\vec{r}')dv'\,dv + \frac{1}{2}\int_{\text{cell volume}}\int [n(\vec{r})-n(\vec{r}')]^2 f(\vec{r},\vec{r}')dv\,dv'\right.}{\int_{\text{cell volume}} n^2(\vec{r})dv}.$$

Thus the expression

$$\tau_a = A\left(\frac{N_{0X}}{\xi_X N_{0X}+\xi_Y N_{0Y}}\right)^{1/2}$$

still remains valid for any geometrical configuration as long as the following assumptions hold: the medium is optically thick, and pressure broadening and complete redistribution in frequency prevail.

[1] Y. Salamero, A. Birot, H. Brunet, J. Galy, and P. Millet, J. Chem. Phys. **80**, 4774 (1984).
[2] Y. Salamero, A. Kerdoussi, A. Birot, and P. Millet, J. Phys. B **23**, 3569 (1990).
[3] P. Berejny, P. Millet, M. Saissac, and Y. Salamero, J. Phys. B **26**, 3339 (1993).
[4] A. Gedanken, J. Jortner, B. Raz, and A. Szoke, J. Chem. Phys. **57**, 3456 (1972).
[5] J. Xu and D. W. Setser, J. Chem. Phys. **92**, 4191 (1990).
[6] P. Laporte, P. Gurtler, E. Morikuwa, R. Reininger, and V. Saile, Europhys. Lett. **9**, 533 (1989).
[7] M. G. Payne, J. E. Talmage, G. S. Hurst, and E. B. Wagner, Phys. Rev. A **9**, 1050 (1974).
[8] F. Vermeersch, N. Schoon, E. Desoppere, and W. Wieme, in *Optogalvanic Spectroscopy*, edited by R. S. Stewart and J. E. Lawler, IOP Conf. Proc. No. 113 (Institute of Physics and Physical Society, Bristol, 1991), p. 133.
[9] T. Holstein, Phys. Rev. **72**, 1212 (1947).
[10] T. Holstein, Phys. Rev. **83**, 1159 (1951).
[11] M. G. Payne and J. D. Cook, Phys. Rev. A **2**, 1238 (1970).
[12] K. Igarashi, S. Mikoshiba, Y. Watanabe, M. Suzuki, and S. Muruyama, J. Phys. D **28**, 1377 (1995).
[13] L. M. Biberman and J. Aksperim, Zh. Eksp. Teor. Fiz. **17**, 416 (1947) [Sov. Phys. JETP **19**, 584 (1949)].

[14] A. F. Molisch, B. P. Oehry, and G. Margel, J. Quant. Spectrosc. Radiat. Transf. **48**, 377 (1992).
[15] C. G. Carrington, D. N. Stacey, and J. Cooper, J. Phys. B **6**, 417 (1973).
[16] I. I. Sobel'man, L. A. Valenstein, and E. A. Yukov, *Excitation of Atoms and Broadening of Spectral Lines* (Springer-Verlag, Berlin, 1981).
[17] E. Matthias, R. A. Rosenberg, E. D. Poliakoff, M. G. White, S. T. Lee, and D. A. Shirley, Chem. Phys. Lett. **52**, 239 (1977).
[18] A. Omont, C. R. Seances Acad. Sci., Ser. B **262**, 190 (1966).
[19] H. Margenau and W. W. Watson, Rev. Mod. Phys. **8**, 22 (1936).
[20] W. Furssow and A. Wlassow, Phys. Z. Sowjetunion **10**, 379 (1936).
[21] E. Lindholm, Ark. Mat., Astron. Fys. **A32**, 17 (1945).
[22] H. M. Foley, Phys. Rev. **69**, 616 (1946).
[23] F. W. Byron, Jr. and H. M. Foley, Phys. Rev. **134**, A625 (1964).
[24] A. Omont and J. Meunier, Phys. Rev. **169**, 92 (1968).
[25] A. P. Kazantsev, Zh. Eksp. Teor. Fiz. **51**, 1751 (1966) [Sov. Phys. JETP **24**, 1183 (1967)].
[26] H. Nowotny, Phys. Lett. **36A**, 481 (1971).
[27] P. R. Berman and W. E. Lamb, Jr., Phys. Rev. **187**, 221 (1969).

[28] C. A. Mead, Int. J. Theor. Phys. **1**, 317 (1968).

[29] Yu. A. Vdovin and V. M. Galitskii, Zh. Eksp. Teor. Fiz. **52**, 1345 (1967) [Sov. Phys. JETP **25**, 894 (1967)].

[30] J. M. Vaughan, Phys. Lett. **21**, 153 (1966).

[31] J. W. Hutcherson and P. M. Griffin, J. Opt. Soc. Am. **63**, 338 (1973).

[32] N. P. Penkin and L. N. Shabanova, Opt. Spectrosc. **26**, 191 (1969).

[33] D. Perrin-Lagarde and R. Lennuier, J. Phys. (Paris) **36**, 357 (1975).

[34] V. V. Skidan and E. Ya. Shreider, Opt. Spectrosc. **28**, 340 (1970).

[35] J. P. Gardou, Ph.D. thesis, University Paul Sabatier, 1998.

[36] F. Marchal, Ph.D. thesis, University Paul Sabatier, 1996.

[37] Y. Salamero, Ph.D. thesis, University Paul Sabatier, 1984.

[38] A. Kerdoussi, Ph.D. thesis, University Paul Sabatier, 1989.

[39] J. N. Foulquier, Ph.D. thesis, University Paul Sabatier, 1986.

[40] M. Rouzaud, Ph.D. thesis, University Paul Sabatier, 1986.

[41] E. Audouard, P. Laporte, J. L. Subtil, and N. Damany, J. Chem. Phys. **89**, 6176 (1988).

[42] T. D. Bonifield, F. H. K. Rambow, G. K. Walters, M. V. Mc Cusker, D. C. Lorents, and R. A. Gutcheck, Chem. Phys. Lett. **69**, 290 (1980).

[43] P. K. Leichner, K. F. Palmer, J. D. Cook, and M. Thieneman, Phys. Rev. A **13**, 1787 (1976).

[44] R. Broadman and G. Zimmerer, Chem. Phys. Lett. **56**, 434 (1978).

[45] J. P. Montagne, Ph.D. thesis, University Paul Sabatier, 1979.

[46] H. Janssens, M. Vanmarcke, E. Desopere, J. Lenaerts, R. Boucique, and W. Wieme, J. Chem. Phys. **86**, 4925 (1987).

[47] C. Van Trigt, Phys. Rev. **181**, 97 (1969).

[48] J. E. Lawler, G. J. Parker, and W. N. G. Hitchon, J. Quant. Spectrosc. Radiat. Transf. **49**, 627 (1993).

[49] J. C. Molino Garcia, W. Bötticher, and M. Kock, J. Quant. Spectrosc. Radiat. Transf. **55**, 169 (1996).

[50] W. F. Chan, G. Cooper, X. Guo, G. R. Burton, and C. E. Brion, Phys. Rev. A **46**, 149 (1992); **48**, 858(E) (1993).

[51] T. Takayanagi, G. P. Li, K. Wakiya, H. Suzuki, T. Ajiro, T. Iniba, S. S. Kano, and T. Takuma, Phys. Rev. A **41**, 5948 (1990).

[52] S. Tsurubuchi, K. Watanabe, and T. Arikawa, J. Phys. Soc. Jpn. **59**, 1947 (1990).

[53] P. Laporte and H. Damany, J. Phys. **40**, 9 (1979).

[54] R. Turner, Phys. Rev. **140**, A426 (1965).

[55] R. C. G. Ligtenberg, P. J. M. Van der Burgt, S. P. Renwick, W. B. Westerveld, and J. S. Risley, Phys. Rev. A **49**, 2363 (1994).

[56] N. D. Gibson and J. S. Risley, Phys. Rev. A **52**, 4451 (1995).

[57] A. Delage and J. D. Carette, Phys. Rev. B **9**, 2399 (1976).

[58] J. Geiger, Phys. Lett. **33A**, 351 (1970); Z. Phys. A **129**, 282 (1977).

[59] P. M. Griffin and J. W. Hutcherson, J. Opt. Soc. Am. **59**, 1607 (1969); **61**, 136(E) (1970).

[60] J. M. Vaughan, Phys. Rev. **166**, 13 (1968).

[61] G. I. Chaschina and E. Y. Shreider, Opt. Spectrosc. **22**, 284 (1967).

[62] P. G. Wilkinson, J. Quant. Spectrosc. Radiat. Transf. **5**, 503 (1965).

[63] E. L. Lewis, Proc. Phys. Soc. London **92**, 817 (1967).

[64] G. I. Chaschina and E. Y. Shreider, Opt. Spectrosc. **20**, 283 (1966).

[65] P. G. Wilkinson, J. Quant. Spectrosc. Radiat. Transf. **6**, 823 (1966).

[66] W. Wieme and P. Mortier, Physica (Amsterdam) **65**, 198 (1973).

[67] A. Delage and J. D. Carette, Phys. Rev. A **14**, 1345 (1976).

[68] D. K. Anderson, Phys. Rev. **137**, A21 (1965).

[69] H. M. Anderson, S. D. Bergeson, D. A. Doughty, and J. E. Lawler, Phys. Rev. A **51**, 211 (1995).

[70] W. Wieme and M. Vanmarcke, Phys. Lett. A **72**, 215 (1979).

[71] P. L. Smith, G. G. Lombardi, B. L. Cardon, and W. H. Parkinson, Appl. Opt. **20**, 647 (1981).

[72] W. R. Ferrel, M. G. Payne, and W. R. Garrett, Phys. Rev. A **35**, 5020 (1987).

[73] T. Y. Suzuki, Y. Sakai, B. S. Min, T. Takayanagi, K. Wakiya, H. Suzuki, T. Iniba, and H. Takuma, Phys. Rev. A **43**, 5867 (1991).

[74] J. Keto, R. E. Gleason, T. D. Bonifield, G. K. Walters, and F. K. Soley, Chem. Phys. Lett. **42**, 125 (1976).

[75] T. D. Bonifield, F. H. K. Rambow, G. K. Walters, M. V. Mc Custer, D. C. Lorents, and R. A. Gutcheck, J. Chem. Phys. **72**, 5 (1980); **72**, 2915 (1980).

[76] D. Haaks and K. H. Becker (private communication).

[77] R. Brodmann and G. Zimmerer, J. Phys. B **10**, 3395 (1977).

[78] H. Brunet, A. Birot, H. Dijols, J. Galy, P. Millet, and Y. Salamero, J. Phys. B **15**, 2945 (1982).

[79] M. Vanmarcke, Ph.D. thesis, Gant 1981.

[80] W. Wieme, M. Vanmarcke, and W. Bruynooghe, J. Phys. (Paris), Colloq. **40**, C7-3 (1979).

[81] F. Vermeersch and W. Wieme, in *Optogalvanic Spectroscopy* (Ref. [8]), p. 109.

[82] H. Lange and F. Leipold, Contrib. Plasma Phys. **37**, 377 (1997).

[83] A. Barbet, N. Sadeghi, and J. C. Pebay-Peyroula, J. Phys. B **8**, 1776 (1975).

[84] P. Millet, A. Birot, H. Brunet, J. Galy, B. Pons-Germain, and J. L. Teyssier, J. Chem. Phys. **69**, 92 (1978).

[85] P. R. Timpson and J. M. Anderson, Can. J. Phys. **48**, 1817 (1970).

[86] C. J. Tracy, R. C. Brindle, and H. J. Oskam, J. Chem. Phys. **68**, 4381 (1978).

[87] H. D. Wenck, S. S. Hasnain, M. M. Nikitin, K. Sommer, G. Sommerer, and D. Haaks, Chem. Phys. Lett. **66**, 138 (1979).

[88] W. Wieme, J. Phys. B **7**, 850 (1974).

[89] A. W. Ali and H. R. Griem, Phys. Rev. **140**, A1044 (1965); Phys. Rev. **144**, 366(E) (1966).

[90] A. G. Belov, A. D. Klementov, S. A. Pendyur, I. Ya Fugol, and E. M. Yurtaeva, Opt. Spektrosk. **61**, 961 (1986) [Opt. Spectrosc. **61**, 601 (1986)].

[91] S. Kubodera, M. Honda, M. Kitahara, J. Kawanaka, W. Sasaki, and K. Kurosawa, Jpn. J. Appl. Phys. **34**, 618 (1995).

[92] P. Berejny, Ph.D. thesis, University Paul Sabatier, 1993.

[93] J. D. Cook and P. K. Leichner, Phys. Rev. A **43**, 1614 (1991).

[94] R. E. Gleason, T. D. Bonifield, J. W. Keto, and G. K. Walters, J. Chem. Phys. **66**, 1589 (1977).

[95] J. K. Rice and A. W. Johnson, J. Chem. Phys. **63**, 5235 (1975).